



This is a repository copy of *Coexistence of multiple globin genes conferring protection against nitrosative stress to the Antarctic bacterium Pseudoalteromonas haloplanktis TAC125*.

White Rose Research Online URL for this paper:  
<http://eprints.whiterose.ac.uk/125967/>

Version: Accepted Version

---

**Article:**

Coppola, D., Giordano, D., Milazzo, L. et al. (6 more authors) (2018) Coexistence of multiple globin genes conferring protection against nitrosative stress to the Antarctic bacterium *Pseudoalteromonas haloplanktis* TAC125. *Nitric Oxide*, 73. pp. 39-51.

<https://doi.org/10.1016/j.niox.2017.12.006>

---

**Reuse**

This article is distributed under the terms of the Creative Commons Attribution-NonCommercial-NoDerivs (CC BY-NC-ND) licence. This licence only allows you to download this work and share it with others as long as you credit the authors, but you can't change the article in any way or use it commercially. More information and the full terms of the licence here: <https://creativecommons.org/licenses/>

**Takedown**

If you consider content in White Rose Research Online to be in breach of UK law, please notify us by emailing [eprints@whiterose.ac.uk](mailto:eprints@whiterose.ac.uk) including the URL of the record and the reason for the withdrawal request.



[eprints@whiterose.ac.uk](mailto:eprints@whiterose.ac.uk)  
<https://eprints.whiterose.ac.uk/>

1 **Coexistence of multiple globin genes conferring protection against nitrosative stress to the**  
2 **Antarctic bacterium *Pseudoalteromonas haloplanktis* TAC125**

3  
4 **Daniela Coppola<sup>a</sup>, Daniela Giordano<sup>a,b</sup>, Lisa Milazzo<sup>c</sup>, Barry D. Howes<sup>c</sup>, Paolo Ascenzi<sup>d</sup>,**  
5 **Guido di Prisco<sup>a</sup>, Giulietta Smulevich<sup>c</sup>, Robert K. Poole<sup>e</sup>, Cinzia Verde<sup>a,b,f\*</sup>**

6  
7 <sup>a</sup>Institute of Biosciences and BioResources (IBBR), CNR, Via Pietro Castellino 111, I-80131  
8 Naples, Italy

9 <sup>b</sup>Stazione Zoologica Anton Dohrn, Villa Comunale, Naples, Italy

10 <sup>c</sup>*Department of Chemistry ‘Ugo Schiff’, University of Firenze, Via della Lastruccia 3-13, I-50019*  
11 *Sesto Fiorentino (Fi), Italy*

12 <sup>d</sup>Interdepartmental Laboratory for Electron Microscopy, Roma Tre University, Via della Vasca  
13 Navale 79, I-00146 Rome, Italy

14 <sup>e</sup>Department of Molecular Biology & Biotechnology, The University of Sheffield, S10 2TN, UK

15 <sup>f</sup>Department of Biology, Viale Marconi 448, Roma Tre University, I-00146 Rome, Italy

16  
17 **Running title:** The role of bacterial globins in the Antarctic environment

18

19

20 **\*Corresponding author:**

21 Cinzia Verde

22 E-mail: [c.verde@ibp.cnr.it](mailto:c.verde@ibp.cnr.it); [cinzia.verde@ibbr.cnr.it](mailto:cinzia.verde@ibbr.cnr.it)

23

24 **Abstract**

25 Despite the large number of globins recently discovered in bacteria, our knowledge of their  
26 physiological functions is restricted to only a few examples. In the microbial world, globins appear  
27 to perform multiple roles in addition to the reversible binding of oxygen; all these functions are  
28 attributable to the heme pocket that dominates functional properties. Resistance to nitrosative stress  
29 and involvement in oxygen chemistry seem to be the most prevalent functions for bacterial globins,  
30 although the number of globins for which functional roles have been studied via mutation and  
31 genetic complementation is very limited. The acquisition of structural information has considerably  
32 outpaced the physiological and molecular characterisation of these proteins.

33 The genome of the Antarctic cold-adapted bacterium *Pseudoalteromonas haloplanktis*  
34 TAC125 (PhTAC125) contains genes encoding three distinct single-chain 2/2 globins, supporting  
35 the hypothesis of their crucial involvement in a number of functions, including protection against  
36 oxidative and nitrosative stress in the cold and O<sub>2</sub>-rich environment. In the genome of PhTAC125,  
37 the genes encoding 2/2 globins are constitutively transcribed, thus suggesting that these globins are  
38 not functionally redundant in their physiological function in PhTAC125. In the present study, the  
39 physiological role of one of the 2/2 globins, Ph-2/2HbO-2217, was investigated by integrating in  
40 vivo and in vitro results. This role includes the involvement in the detoxification of reactive nitrogen  
41 and O<sub>2</sub> species including NO by developing two in vivo and in vitro models to highlight the  
42 protective role of Ph-2/2HbO-2217 against reactive nitrogen species. The PSHAa2217 gene was  
43 cloned and over-expressed in the flavohemoglobin-deficient mutant of *Escherichia coli* and the  
44 growth properties and O<sub>2</sub> uptake in the presence of NO of the mutant carrying the PSHAa2217 gene  
45 were analysed. The ferric form of Ph-2/2HbO-2217 is able to catalyse peroxynitrite isomerisation in  
46 vitro, indicating its potential role in the scavenging of reactive nitrogen species. Here we present in  
47 vitro evidence for the detoxification of NO by Ph-2/2HbO-2217.

48 **Keywords:** Antarctic cold-adapted bacterium; bacterial globin; nitrosative/oxidative stress;  
49 Resonance Raman spectroscopy.

## 50 **1. Introduction**

51 Many bacterial genomes contain genes encoding more than a single globin and there is a  
52 strong correlation between the number of globin genes and the genome size (Giovannoni et al.,  
53 2005). Globins are classified in three families: (i) myoglobin (Mb)-like proteins (M), displaying the  
54 classical three-on-three (3/3)  $\alpha$ -helical sandwich motif; (ii) sensor globins (S), and (iii) truncated (T)  
55 hemoglobins (Hbs), showing the two-on-two (2/2)  $\alpha$ -helical-sandwich motif (Vinogradov et al.,  
56 2013). Members of the T family (also known as 2/2Hbs) are found in eubacteria, cyanobacteria,  
57 protozoa, and plants, but not in animals (Wittenberg et al., 2002; Milani et al., 2005; Vinogradov et  
58 al., 2013). On the basis of phylogenetic analysis, the T family can be further divided into three  
59 distinct sub-families/groups: HbI (or N), HbII (or O) and HbIII (or P), with a novel, small (4%)  
60 clade of sequences named HbIV (or Q) that contains only bacterial sequences (Bustamante et al.,  
61 2016).

62 Some of the organisms hosting the 2/2Hbs are pathogenic bacteria; others perform  
63 photosynthesis, fix nitrogen or may display distinctive metabolic capabilities (Pesce et al., 2013,  
64 and refs therein). Some proposed functions include protection from reactive oxygen and nitrogen  
65 species (ROS and RNS, respectively), O<sub>2</sub> and sulfide chemistry (Pesce et al., 2013, and refs therein;  
66 Boubeta et al., 2016). In fact, recent genome analyses (Vinogradov et al., 2013; Bustamante et al.,  
67 2016) reveal a preponderance of 2/2Hbs in cyanobacteria and green algae, and phylogeny supports  
68 the rise of these globins after the appearance of life about 3 billion years ago (Vinogradov et al.,  
69 2006). Since the 2/2Hbs scaffold probably evolved before the development of the current aerobic  
70 environment, a putative original role for these proteins could have been that of O<sub>2</sub> detoxification  
71 following the increase of O<sub>2</sub> levels and the evolution of photosynthesis (Crowe et al., 2013). The  
72 search for globin physiological functions is further driven by the evidence that many 2/2Hbs are  
73 capable of reacting with NO, nitrite, and peroxyxynitrite (Gardner, 2005; Ascenzi et al., 2009; De  
74 Marinis et al., 2009; Ascenzi et al., 2014; Pesce et al., 2016). Interestingly, an unusual occurrence of  
75 the concomitant presence of 2/2Hbs of group II and flavohemoglobin (Fhb) in the same genome

76 has been demonstrated (Vinogradov et al., 2013). These findings might indicate that the function of  
77 the 2/2Hbs of group II can be intimately linked to the well-known function of FHb in NO  
78 detoxification (Gardner et al., 1998; Membrillo-Hernández et al., 1999; Mills et al., 2001; Stevanin  
79 et al., 2000). In some cases, 2/2Hbs from more than one group can coexist in the same organism,  
80 indicating diversification of their functions (Vinogradov et al., 2013). The 2/2Hbs have amino-acid  
81 sequences either shorter or longer than those of  $\alpha$  and  $\beta$  globins and Mb (i.e. less than 130 and more  
82 than 160 residues, respectively).

83 The most striking differences between the 2/2 and the 3/3 globin folds are: (i) the drastically  
84 shortened helix A; (ii) the severe alteration of the C-E region; (iii) the presence of a long  
85 polypeptide segment (pre-F) in extended conformation, and (iv) a variable-length helix F that  
86 effectively supports the proximal HisF8 residue coordinated to the heme Fe atom (Pesce et al.,  
87 2013).

88 A distinct aspect of groups I and II is the presence of cavities inside the structure linking the  
89 protein surface to the distal heme, responsible for storage and diffusion of ligands to/from the heme.  
90 The 2/2Hbs generally display moderate to very low O<sub>2</sub>-dissociation rates, and thus moderate to high  
91 O<sub>2</sub> affinity, due to the presence of at least one hydrogen-bond between the heme Fe-bound ligand  
92 and the protein matrix, most commonly provided by TyrB10, TrpG8, His or Tyr at CD1 and  
93 GlnE11 (Pesce et al., 2013; Bustamante et al., 2016).

94 The genome of the cold-adapted bacterium *Pseudoalteromonas haloplanktis* TAC125  
95 (PhTAC125) contains multiple genes encoding three distinct 2/2Hbs (Giordano et al., 2007),  
96 supporting the hypothesis of their involvement in several functions, including protection against  
97 oxidative and nitrosative stress in the cold and O<sub>2</sub>-rich environment of Antarctica. In particular,  
98 PhTAC125 also hosts one 2/2HbI (encoded by the PSHAa0458 gene), two distinct 2/2Hbs of group  
99 II (Ph-2/2HbO-0030 and Ph-2/2HbO-2217, encoded by the PSHAa0030 and PSHAa2217 genes,  
100 respectively), and one FHb, annotated as PSHAa2880 (Giordano et al., 2007). It is worth noting that

101 Ph-2/2HbO-0030 and Ph-2/2HbO-2217 are both endowed with hexa-coordination (Giordano et al.,  
102 2011; Howes et al., 2011; Russo et al., 2013; Giordano et al., 2015; this study).

103 Ph-2/2HbO-0030 has been extensively characterised by spectroscopic analysis, kinetic  
104 measurements, computer simulation and X-ray crystallography by some of the present authors  
105 (Howes et al., 2011; Giordano et al., 2011, 2013, 2015; Russo et al., 2013). The results indicate  
106 unique adaptive structural properties that enhance the overall flexibility of the protein (Giordano et  
107 al., 2015). Recent results on a genomic mutant strain highlight the involvement of cold-adapted Ph-  
108 2/2HbO-0030 in protection against stresses induced by high O<sub>2</sub> concentration (Parrilli et al., 2010)  
109 and RNS (Coppola et al., 2013).

110 In the genome of PhTAC125, two 2/2 globins Ph-2/2HbO-0030 and Ph-2/2HbO-2217  
111 encoding genes are constitutively transcribed, thus suggesting that these 2/2Hbs are not functionally  
112 redundant in their physiological function in PhTAC125. Thus, the putative role of the Ph-2/2HbO-  
113 2217 globin was investigated in the present study by integrating in vivo and in vitro results, with the  
114 aim of shedding light on its physiological role, with special attention to involvement in the RNS  
115 detoxification mechanisms, in the context of analyzing specific functional hypotheses.

116 The PSHAa2217 gene was cloned and over-expressed in the FHb-deficient mutant of  
117 Escherichia coli and the growth properties and O<sub>2</sub> uptake in the presence of NO of the mutant  
118 carrying the PSHAa2217 gene were analysed. The ferric form of Ph-2/2HbO-2217 is able to  
119 catalyse peroxynitrite isomerisation in vitro, indicating its potential role in the scavenging of RNS.  
120 Here we present in vitro evidence for the detoxification of NO by Ph-2/2HbO-2217.

121

## 122 **2. Materials and Methods**

123

### 124 2.1. Sequence alignment

125 Sequence alignment was performed by the program CLUSTAL OMEGA and manual  
126 adjustments were based on known crystal structures. The 2/2Hbs belonging to Group II are: Ph-

127 2/2HbO-2217, Ph-2/2HbO-0030 (Giordano et al., 2015), *Thermobifida fusca* (Tf-2/2HbO)  
128 (Bonamore et al., 2005), *Mycobacterium tuberculosis* (Mt-2/2HbO) (Milani et al., 2003), *M. leprae*  
129 (Ml-2/2HbO) (Visca et al., 2002), *Agrobacterium tumefaciens* (At-2/2HbO) (Pesce et al., 2011),  
130 *Bacillus subtilis* (Bs-2/2HbO) (Giangiacomo et al., 2005), and *Geobacillus stearothermophilus* (Gs-  
131 2/2HbO) (Ilari et al., 2007). The homology model of Ph-2/2HbO-2217, using the 3D-structure  
132 (PDB ID 4UUR) of Ph-2/2HbO-0030 as template, was built with SwissModel  
133 (<https://swissmodel.expasy.org/>) (Arnold et al., 2006, 2011; Biasini et al., 2014).

134

## 135 2.2. Strains and culture conditions

136 Since the FHb (Hmp) from *E. coli* provides a highly effective detoxification mechanism for  
137 NO, we used strain RKP3036 (carrying a genomic hmp null mutation) for cloning and expressing the  
138 PSHAa2217 gene, to test cell survival and O<sub>2</sub> uptake in the presence of nitrosative stress. *E. coli*  
139 RKP3919 (*E. coli* RKP3036 carrying the empty vector pBAD/HisA) was used as a negative control.  
140 *E. coli* RKP3910 strain [*E. coli* RKP3036 transformed with the pPL341 vector carrying the wild-  
141 type hmp<sup>+</sup> gene (Vasudevan et al., 1991)] and *E. coli* RKP3036 carrying the PSHAa0030 gene  
142 (Coppola et al., 2013) were used as positive controls. The *E. coli* TOP10 strain was used for cloning  
143 and expressing the PSHAa2217 gene, and to purify the protein Ph-2/2HbO-2217. Cells were grown  
144 in Luria-Bertani (LB) medium, pH 7.0, at 25 °C, 180 rpm and under aerobic conditions. When  
145 required, ampicillin (Amp, 100 µg/mL) and kanamycin (Km, 35 µg/mL) were added.

146

## 147 2.3. Cloning and expression of the PSHAa2217 gene

148 The primer pairs forward (5'-TATGAGTGAGCCATGGATACTAAAGT-3') and reverse (5'-  
149 GCGGGATCCCTAGCTACCCGATACCATTCT-3') were designed on the basis of the  
150 PSHAa2217 gene sequence encoding Ph-2/2HbO-2217 (Médigue et al., 2005). The sequence  
151 corresponding to the NcoI site was introduced in the forward primer. The PSHAa2217 gene was  
152 retrieved from the genomic DNA of PhTAC125 using the PCR approach. The amplified fragment

153 was directly cloned into the pTZ57R/T vector and sequenced to verify its authenticity.

154 The NcoI-PstI digested fragment of the PSHAa2217 gene was further cloned into the  
155 corresponding sites of the L-arabinose-inducible, Amp-resistant, and His-tagged pBAD/HisA vector  
156 (Invitrogen, Carlsbad, CA, USA). The restriction enzyme cut-sites (NcoI and PstI) were designed  
157 for the insertion of the PSHAa2217 gene in pBAD/HisA without the His-tagged region. The  
158 construction was verified by sequencing and named pBAD-2/2HbO-2217.

159 For over-expression of the globin gene in the E. coli hmp mutant and in E. coli TOP10, the  
160 cells were transformed with plasmid construct pBAD-2/2HbO-2217 and inoculated into LB  
161 medium supplemented with Amp (100 µg/mL). For growth of the E. coli hmp mutant, Km (35  
162 µg/mL) was also added to the medium. Cells were allowed to grow at 25 °C until  $A_{600}$  reached ~ 1  
163 OD and then supplemented with 0.2 mM  $\delta$ -aminolevulinic acid, 0.012 mM FeCl<sub>3</sub>, and 0.06% L-  
164 arabinose, and further incubated for 5 h at 25 °C. Expression of the globin was monitored by  
165 running the cell lysate of recombinant strains on 15% SDS-PAGE followed by Coomassie Brilliant  
166 Blue staining.

167

#### 168 2.4. Protein purification

169 Purification of Ph-2/2HbO-2217 was achieved by FPLC (GE Healthcare Biosciences,  
170 Amersham Biosciences Ltd, UK) anion-exchange chromatography, loading the cell lysate obtained  
171 from E. coli TOP10 expressing the PSHAa2217 gene on a Q Sepharose column (HiTrap™ QFF, GE  
172 Healthcare Biosciences, Amersham Biosciences Ltd, UK), equilibrated with 20 mM Tris-HCl pH  
173 8.2. Ph-2/2HbO-2217 was eluted with a NaCl gradient from 0 to 1.0 M. The eluate was further  
174 purified by a second anion-exchange chromatography step on a Mono Q-Tricorn column,  
175 equilibrated with 20 mM Tris-HCl pH 8.2. The protein was eluted with a NaCl gradient from 0 to  
176 250 mM. All buffers were prepared in MilliQ water. The protein obtained was > 98% pure on SDS-  
177 PAGE. The N-terminal sequence was determined by automatic sequencing performed with an  
178 Applied Biosystems Procise 494 automatic sequencer, equipped with on-line detection of



179 phenylthiohydantoin amino acids.

180

## 181 2.5. Samples for spectroscopic analysis

182 Ferric Ph-2/2HbO-2217 at pH 6.0, 7.6 and 9.9 was prepared in 50 mM MES [2-(N-  
183 morpholino) ethanesulfonic acid], 20 mM Tris-HCl and 50 mM glycine, respectively. The hydroxyl  
184 complex in isotopically enriched water was prepared by washing Ph-2/2HbO-2217 in 20 mM Tris-  
185 HCl pH 7.6 with 0.1 mM glycine pD 10.2 prepared with D<sub>2</sub>O (99.8%) (Merck AG Darmstadt,  
186 Germany). Ferrous samples at pH 7.6 were prepared by addition of a freshly prepared sodium  
187 dithionite solution (10 mg/mL) to the ferric forms previously flushed with nitrogen. The Fe(II)-CO  
188 complex at pH 7.6 was prepared by flushing ferric Ph-2/2HbO-2217 firstly with nitrogen, then with  
189 <sup>12</sup>CO or <sup>13</sup>CO (Rivoira, Milan, Italy), and reducing the heme by addition of a freshly prepared  
190 sodium dithionite solution (10 mg/mL). All chemicals were of analytical or reagent grade and were  
191 used without further purification.

192 Protein concentration in the range 10–30 μM was used for electronic absorption and  
193 Resonance Raman (RR) spectroscopies at both room and low temperature. The concentration used  
194 for Electron Paramagnetic Resonance (EPR) spectroscopy was 100 μM. The protein concentration  
195 was estimated on the basis of the molar absorptivity of the ferric form at 408 nm,  $\epsilon = 131 \text{ mM}^{-1}$   
196  $\text{cm}^{-1}$ .

197

## 198 2.6. Electronic absorption measurements

199 UV-visible absorption spectra of whole cells of *E. coli* hmp carrying pBAD/HisA and pBAD-  
200 2/2HbO-2217 were recorded using an SDB-4 dual-wavelength scanning spectrophotometer  
201 (University of Pennsylvania Biomedical Instrumentation Group, and Current Designs, Inc.,  
202 Philadelphia, PA) at room temperature (Kalnenieks et al., 1998). Samples were generally scanned  
203 with a 0.5-nm step size. Data were analysed using SoftSDB (Current Designs) and Sigma Plot 11.0  
204 (Systat Software, Inc., San Jose, CA, USA).

205 Aerobic cultures were grown overnight (for about 18 h) in flasks containing medium up to 1/5  
206 of their volume with appropriate antibiotics and supplements in different concentrations. Cells were  
207 harvested by spinning at 5500 rpm for 15 min at 4 °C and the pellets were re-suspended in 6 mL of  
208 0.1 M sodium phosphate buffer, pH 7.0. Spectra were recorded between 400 nm and 700 nm. All  
209 spectra were baseline-corrected.

210 UV-visible absorption spectra of cell lysates of *E. coli hmp* carrying either pBAD/HisA or  
211 pBAD-2/2HbO-2217 were measured with a double-beam Cary 300 spectrophotometer (Agilent  
212 Technologies, Santa Clara, CA, USA), using a 120-nm/min scan rate. Pellets, prepared as already  
213 described, were re-suspended in 50 mM Tris-HCl buffer pH 7.4, containing 2 mM MgCl<sub>2</sub> and 1  
214 mM EGTA; cells were disrupted by sonication. The debris was pelleted by centrifugation at  
215 12,000×g for 15 min and membranes recovered from the supernatant by ultracentrifugation for 1 h  
216 at 225,000×g, 4 °C. The absorption spectra of the supernatants were recorded between 400 and 700  
217 nm.

218

## 219 2.7. Resonance Raman measurements

220 The RR spectra were obtained at 25 °C using a 5-mm NMR tube by excitation with the  
221 406.7 and 413.1 nm lines of a Kr<sup>+</sup> laser (Innova 300 C, Coherent, Santa Clara, CA, USA), the 514.5  
222 nm line of an Ar<sup>+</sup> laser (Innova 90/5, Coherent), and the 441.6 nm line of a He–Cd laser (Kimmon  
223 IK4121R-G). Back-scattered light from a slowly rotating NMR tube was collected and focused into  
224 a triple spectrometer with spectral resolution as reported elsewhere (Ciaccio et al., 2017). A  
225 cylindrical lens, which focuses the laser beam in the sample to a narrow strip rather than the usual  
226 point, was used to collect the spectra of both the Fe(II)-CO complex and the ferric sample at pH 7.6  
227 in order to avoid photolysis and minimize sample degradation induced by irradiation.

228 The RR spectra were calibrated with indene, n-pentane and carbon tetrachloride as standards  
229 to an accuracy of 1 cm<sup>-1</sup> for intense isolated bands. All RR measurements were repeated several  
230 times under the same conditions to ensure reproducibility. To improve the signal-to-noise ratio, a

231 number of spectra were accumulated and summed only if no spectral differences were noted. All  
232 spectra were baseline-corrected.

233 For the low temperature experiments, a 1.5-cm diameter quartz crucible positioned in a  
234 THMS600 cryostat (Linkam Scientific Instruments, Surrey, UK) containing ~ 100  $\mu$ L frozen  
235 samples at 80 K was used.

236 Absorption spectra recorded using a 5-mm NMR tube (300 nm/min scan rate) or a 1-cm  
237 cuvette (600 nm/min scan rate) at 25 °C by means of a Cary 60 spectrophotometer (Agilent  
238 Technologies, Glostrup, Denmark) (resolution of 1.5 nm), were measured both prior to and after RR  
239 measurements to ensure that no degradation occurred under the experimental conditions used. ~~All~~  
240 ~~spectra were baseline-corrected.~~

241 For the low temperature experiments, a 1.5-cm diameter quartz crucible positioned in a  
242 THMS600 cryostat (Linkam Scientific Instruments, Surrey, UK) containing ~ 100  $\mu$ L frozen  
243 samples at 80 K was used.

244

## 245 2.8. EPR measurements

246 EPR spectra were recorded with an Elexsys E500 (Bruker, Rheinstetten, Germany),  
247 equipped with an NMR gaussmeter and a microwave frequency counter. An ESR 900 cryostat  
248 (Oxford Instruments, Abingdon, UK), was used to obtain low temperatures. Spectra were recorded  
249 under non-saturating conditions at 5 K, 1-mW microwave power and 1-mT modulation amplitude.  
250 The g values were determined by careful visual inspection of the spectra.

251

## 252 2.9. S-nitrosoglutathione and NO-donors

253 Three different agents of nitrosative stress were used, according to the experimental design.  
254 For growth experiments, a source of NO gas was compared with a nitrosating agent. As a source of  
255 NO, DETA-NONOate (Enzo Life Science, Farmingdale, NY, USA) with a half-life of 20 h at 37 °C  
256 and 56 h at 22–25 °C in 0.1 M phosphate buffer pH 7.4 was used; thus NO release and provision to

257 the bacteria were prolonged over several hours. The nitrosating agent S-nitrosoglutathione (GSNO)  
258 was prepared as previously reported (Hart, 1985). It is widely used in microbial growth experiments  
259 because it is moderately stable in aqueous solutions; however, a derived nitrosated dipeptide, S-  
260 nitroso-L-cysteinylglycine, is transported inwards (via the Dpp-encoded dipeptide permease in  
261 certain bacteria) and intracellular transnitrosation reactions ensue (Laver et al., 2012). In contrast, for  
262 short-term respiration experiments designed to test the addition of a bolus of NO, we used Proli-  
263 NONOate (Bioquote Limited, York, UK) with a half-life of 1.8 s at 37 °C in 0.1 M phosphate buffer  
264 pH 7.4. All experiments were performed in triplicate.

265

#### 266 2.10. GSNO and NO susceptibility

267 Cultures of the *E. coli* hmp mutant, transformed with pBAD/HisA (negative control), pBAD-  
268 2/2HbO-0030 (positive control) (Coppola et al., 2013) and pBAD-2/2HbO-2217, were grown in  
269 plastic universal tubes in 2 mL of LB medium containing appropriate antibiotics and incubated for  
270 2.5 h at 25 °C. The culture was then supplemented with: 0.2 mM  $\delta$ -aminolevulinic acid, 0.012 mM  
271 FeCl<sub>3</sub>, L-arabinose at the final concentration of 0.06% for *E. coli* hmp carrying either Ph-2/2HbO-  
272 2217 or the empty vector, and at the final concentration of 0.2% for the positive control *E. coli* hmp  
273 carrying Ph-2/2HbO-0030 (as in Coppola et al., 2013). GSNO and DETA-NONOate were later  
274 added to all tubes at different concentrations (GSNO: 0, 1, 3, and 5 mM; DETA-NONOate: 0, 0.5, 1,  
275 and 2 mM).

276 The cultures were incubated for approximately 18 h in the dark, at 25 °C with shaking, and  
277 then the optical density at 600 nm was recorded.

278

#### 279 2.11. Growth curves

280 Cultures of the *E. coli* hmp carrying different plasmids were grown in the dark in 250 mL  
281 flasks containing 10 mL of medium with appropriate antibiotics. Induction supplements (for details

282 see section on GSNO and NO susceptibility), GSNO (3 mM) or DETA-NONOate (0.5 mM) were  
283 added to each flask, at  $t = 2.5$  h.

284

## 285 2.12. NO uptake and cellular respiration

286 Cultures of the *E. coli* hmp mutant carrying pBAD-2/2HbO-2217, pBAD-2/2HbO-0030, and  
287 pBAD/HisA were grown in 250 mL flasks containing 40 mL of LB medium, supplemented with the  
288 appropriate antibiotics. Induction supplements were added when the cells reached an OD of 1.0.  
289 Cultures were grown overnight (around 18 h), at 25 °C. Cells were harvested at 5500 rpm for 15 min  
290 at 4 °C; the pellets obtained were washed twice with 10 mL 50 mM Tris-HCl buffer pH 7.5, then re-  
291 suspended in 5-10 mL of the same buffer to normalise the optical density (OD) of the suspensions.

292 The respiration rates of whole cells were measured using a Clark-type polarographic O<sub>2</sub>  
293 electrode (Rank Bros, Bottisham, Cambridge, UK) operating at a polarising voltage of 0.60 V. The  
294 apparatus consists of a Perspex chamber kept at 25 °C using a water jacket around the chamber and  
295 stirred magnetically with a membrane-covered electrode placed at the bottom of the chamber  
296 (Stevanin et al., 2000). The electrode was calibrated using air-saturated buffer, which was then  
297 treated with a small amount of sodium dithionite to achieve anoxia. Parallel measurements of O<sub>2</sub> and  
298 NO were made by housing a World Precision Instruments (Sarasota, FL, USA) ISO NOP sensor (2-  
299 mm diameter) in the same vessel (Mills et al., 2001); note that the ingress of air around the NO port  
300 results in slow backflow of O<sub>2</sub> into the chamber contents.

301 The NO electrode was calibrated as described by the manufacturer (World Precision  
302 Instruments, Sarasota, FL, USA). Briefly, sequential volumes of 50 µM NaNO<sub>2</sub> (e.g. 100, 200, 400,  
303 and 800 µL) were added under stirring to 20 mL of 0.1 M H<sub>2</sub>SO<sub>4</sub>/KI, in which the NO electrode was  
304 suspended.

305 After calibration of the O<sub>2</sub> and NO electrodes, the whole cell suspension was diluted with 50  
306 mM Tris-HCl pH 7.5 in the O<sub>2</sub>-electrode chamber to a final volume of 2 mL, and closed with a  
307 tight-fitting lid. The respiration was started using 25 mM glucose. Proliferation (final

308 concentration, 1  $\mu\text{M}$ ) was added through a hole in the vessel lid using a Hamilton syringe, at  
309 progressively lower  $\text{O}_2$  concentrations. Respiration was followed until the chamber became devoid  
310 of  $\text{O}_2$ .

311

### 312 2.13. Heme assay

313 Absorption spectra of sonicated samples (0.6 mL without clarification) containing 0.6 mL of  
314 reagent (0.4 M NaOH, 4.2 M pyridine) were taken in a quartz cuvette (with stopper) and analysed  
315 between 500 and 700 nm using a double-beam Cary 300 spectrophotometer with a 120-nm/min scan  
316 rate. Each sample was reduced by adding small amounts of sodium dithionite followed by gentle  
317 stirring. A sample was used to obtain the oxidised spectrum by addition of potassium ferricyanide.  
318 Difference spectra of reduced vs oxidised forms were obtained; the heme concentration was  
319 calculated from the absorbance difference at 556 and 539 nm for the dithionite-reduced and  
320 ferricyanide-oxidised samples, respectively.

321

### 322 2.14. Peroxynitrite isomerisation

323 Peroxynitrite was obtained from Cayman Chemical Company (Ann Arbor, MI, USA). The  
324 concentration of peroxynitrite was determined spectrophotometrically by measuring the absorbance  
325 at 302 nm ( $\epsilon = 1.705 \times 10^3 \text{ M}^{-1} \text{ cm}^{-1}$ ). The peroxynitrite stock solution ( $2.0 \times 10^{-3} \text{ M}$ ) was diluted  
326 immediately before use with degassed  $1.0 \times 10^{-2} \text{ M}$  NaOH to reach the desired concentration (Bohle  
327 et al., 1996; Koppenol et al., 1996; Herold and Shivashankar, 2003; Herold et al., 2004a; Ascenzi  
328 and Fasano, 2007; Goldstein and Merényi, 2008).

329 Kinetics of peroxynitrite isomerization, by ferric Ph-2/2HbO-2217 and Ph-2/2HbO-0030, in  
330 the absence and presence of cyanide (final concentration,  $5.0 \times 10^{-4} \text{ M}$ ), was recorded at 302 nm ( $\epsilon =$   
331  $1.705 \times 10^3 \text{ M}^{-1} \text{ cm}^{-1}$ ) by rapidly mixing the buffer solution ( $1.0 \times 10^{-1} \text{ M}$  bis-tris-propane buffer, pH  
332 7.4) or the ferric globin solutions (final concentration, 4 to 16  $\mu\text{M}$ ;  $1.0 \times 10^{-1} \text{ M}$  bis-tris-propane  
333 buffer, pH 7.4) with the peroxynitrite solution (final concentration,  $2.5 \times 10^{-4} \text{ M}$ ).

334 In the absence and presence of ferric globins and cyanide, values of the pseudo-first-order rate  
335 constant for peroxynitrite isomerization (i.e.  $k$ ) were determined from the analysis of the time-  
336 dependent absorbance decrease at 302 nm, according to Eq. (1):

$$337 \text{[peroxynitrite]}_t = \text{[peroxynitrite]}_0 \times e^{-k \times t} \quad (1)$$

338 Values of the second-order rate constant for peroxynitrite isomerization by ferric Ph-2/2HbO-  
339 2217 and Ph-2/2HbO-0030 (i.e.,  $k_{on}$ ) and of the first-order rate constant for the spontaneous  
340 conversion of peroxynitrite to nitrate (i.e.  $k_0$ ) were determined from the dependence of  $k_{on}$  on the  
341 ferric globin concentration, according to Eq. (2):

$$342 k = k_{on} \times [\text{Ph-2/2HbO-2217-Fe(III)}] + k_0 \quad (2)$$

343

### 344 3. Results

345

#### 346 3.1. Primary structure

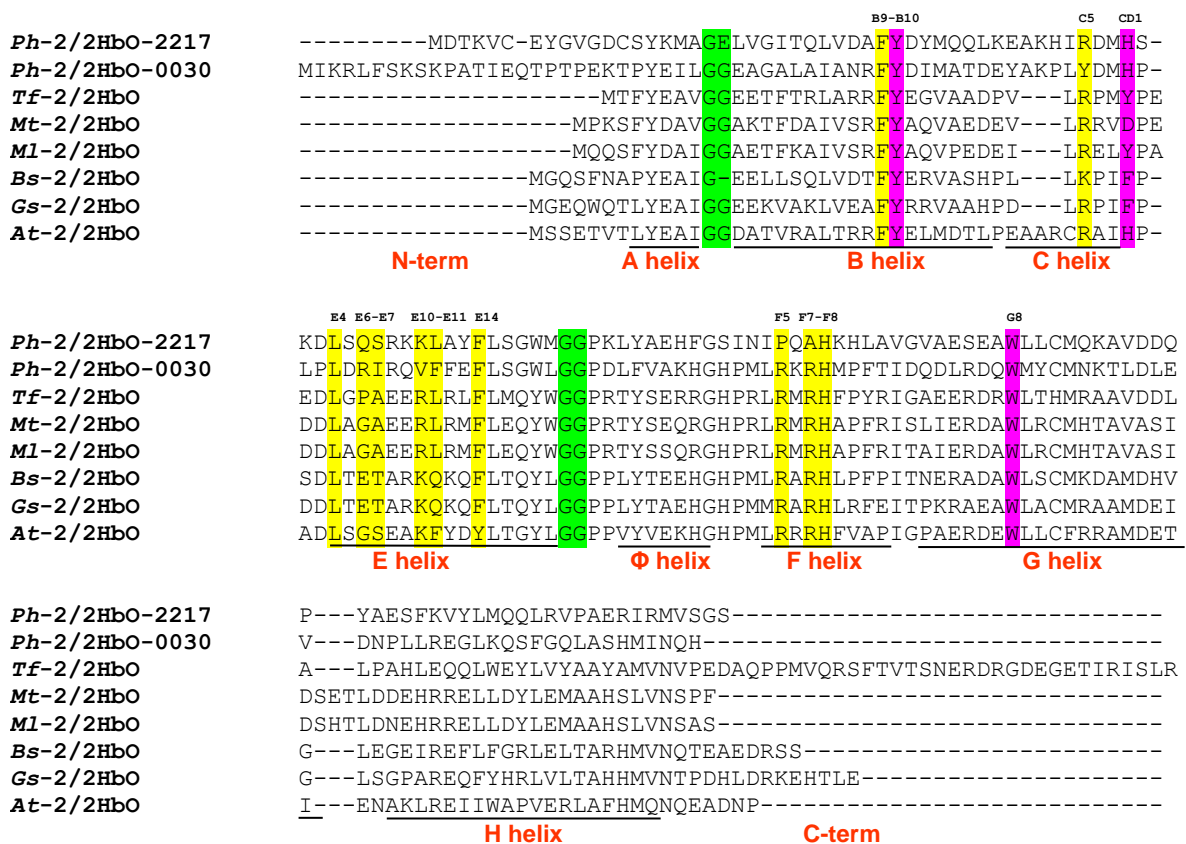
347 **Figure 1A** shows the alignment of Ph-2/2HbO-2217 and Ph-2/2HbO-0030 with some  
348 representative 2/2Hbs belonging to group II. The sequence identity between the two Antarctic  
349 globins is only 24%, thus suggesting that these proteins may play different function(s) in bacterial  
350 physiology.

351 The main difference between Ph-2/2HbO-2217 and Ph-2/2HbO-0030 is the presence in the  
352 former of a longer sequence extension at the N terminus (19 residues in Ph-2/2HbO-0030 and 9  
353 residues in Ph-2/2HbO-2217), rarely observed in 2/2Hbs. In Ph-2/2HbO-0030, the extension is  
354 proteolytically cleaved during protein purification (Giordano et al., 2007), and it does not appear to  
355 be a requirement for NO detoxification (Coppola et al., 2013).

356 By comparison with other group II globins, and taking Mt-2/2HbO as the reference, the two  
357 Antarctic globins show: (i) a three-residue insertion in the BC loop, (ii) one-residue deletion in the  
358 CE loop, (iii) three-residue deletion in the GH loop and at the C terminus (Giordano et al., 2015, this  
359 study), (iv) His and Trp residues at positions F8 and G8, respectively, (v) the Phe-Tyr motif at

360 positions B9-B10, and (vi) a His residue at position CD1. The analysis of all bacterial sequences  
 361 available to date (~ 1100) demonstrated that the CD1 position is occupied predominantly by Phe and  
 362 in some cases by His or Tyr (~ 20 and 15%, respectively) (Bustamante et al., 2016). His (a hydrogen  
 363 bonding residue) at the topological position CD1 site is always matched by a hydrophobic E11  
 364 residue (Leu or Phe). Thus, one of the necessary hydrogen bonding elements involved in ligand  
 365 stabilisation is alternatively located at opposite edges of the heme distal cavity, either at the CD1 or  
 366 at the E11 sites, but never simultaneously. In Ph-2/2HbO-2217, the E11 residue is Leu, while it is  
 367 Phe in Ph-2/2HbO-0030.

368 In Ph-2/2HbO-0030 the two Gly-Gly motifs, located in the AB and EF hinges of 2/2Hbs  
 369 belonging to groups I and II, are present and help to stabilize the short helix A in a conformation  
 370 locked onto helices B and E. In contrast, in Ph-2/2HbO-2217 the second Gly residue is replaced by  
 371 Glu at the AB hinge.



372

373



374 **Figure 1A.** Sequence alignment, carried out by Clustal Omega, of Ph-2/2HbO-2217 and Ph-  
375 2/2HbO-0030 compared with other members of group-II. Manual adjustments have been based on  
376 known crystal structures adapted from Giordano et al. (2015). Functionally important residues are  
377 shown in yellow; residues (B10, CD1 and G8) specific for 2/2Hbs of group-II are in purple; the  
378 Gly-Gly motifs are in green. Helical regions (A-H) are indicated by black bars and helix  $\Phi$ , specific  
379 for 2/2Hb of group-II, is shown. The numbering of residues is based on the position of residues in  
380 the helices of sperm whale Mb, adapted from Giordano et al. (2015).

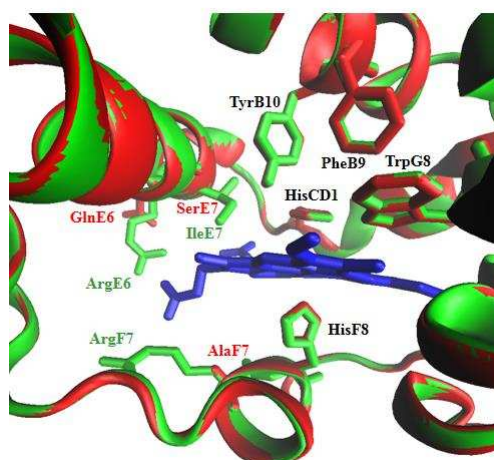
381

382 Position E7 is variable in group II globins and is usually occupied by a small residue (typically  
383 Ala, Ser or Thr), thus suggesting an E7 route entry path to facilitate the accessibility of diatomic  
384 ligands to the heme distal site (Milani et al., 2003; Vuletich and Lecomte, 2006; Nardini et al., 2007;  
385 Pesce et al., 2013). In Ph-2/2HbO-2217, E7 is occupied by Ser (**Figure 1B**), whereas in Ph-2/2HbO-  
386 0030 by Ile, separating the heme distal cavity from the solvent region (Giordano et al., 2015).

387 **Figure 1B** overlays the heme pocket of a Ph-2/2HbO-2217 homology model and the Ph-  
388 2/2HbO-0030 structure used as template, showing different residues involved in the stabilisation of  
389 the heme through Fe coordination. In Ph-2/2HbO-0030, the heme was found to be stabilized through  
390 direct Fe coordination to proximal His(96)F8, electrostatic interactions with the heme propionates,  
391 and van der Waals contacts (< 4.0 Å) with 23 residues. In particular, propionate D is stabilized by an  
392 H-bonded salt bridge with Arg(95)F7, and propionate A is electrostatically coupled to Arg64; in  
393 addition, both propionates are H-bonded with a water molecule (Giordano et al., 2015). However, in  
394 Ph-2/2HbO-2217 the propionate-protein interactions are quite different. In Ph-2/2HbO-2217,  
395 position EF6 is occupied by Tyr (**Figure 1B**), highly conserved in 2/2Hbs of group II (Bustamante et  
396 al., 2016), but not present in Ph-2/2HbO-0030 (Phe was found instead) (Giordano et al., 2015).  
397 Therefore, the formation of an additional H bond with propionate D is predicted. However, Arg at  
398 F7, present in other 2/2Hbs and conserved in Ph-2/2HbO-0030, is replaced by Ala in Ph-2/2HbO-  
399 2217. Moreover, Arg(64)E6, electrostatically coupled to propionate A in Ph-2/2HbO-0030

400 (Giordano et al., 2015), in Ph-2/2HbO-2217 is replaced by Gln.

401



402

403 **Figure 1B.** Superimposition of the heme pocket of a Ph-2/2HbO-2217 homology model (red) and  
404 the Ph-2/2HbO-0030 template structure (green). The heme group is in blue. The residues involved in  
405 the stabilisation of the heme through Fe coordination are shown (B9, B10, CD1, G8, E6, E7, F7, F8),  
406 as reported in Giordano et al. (2015).

407

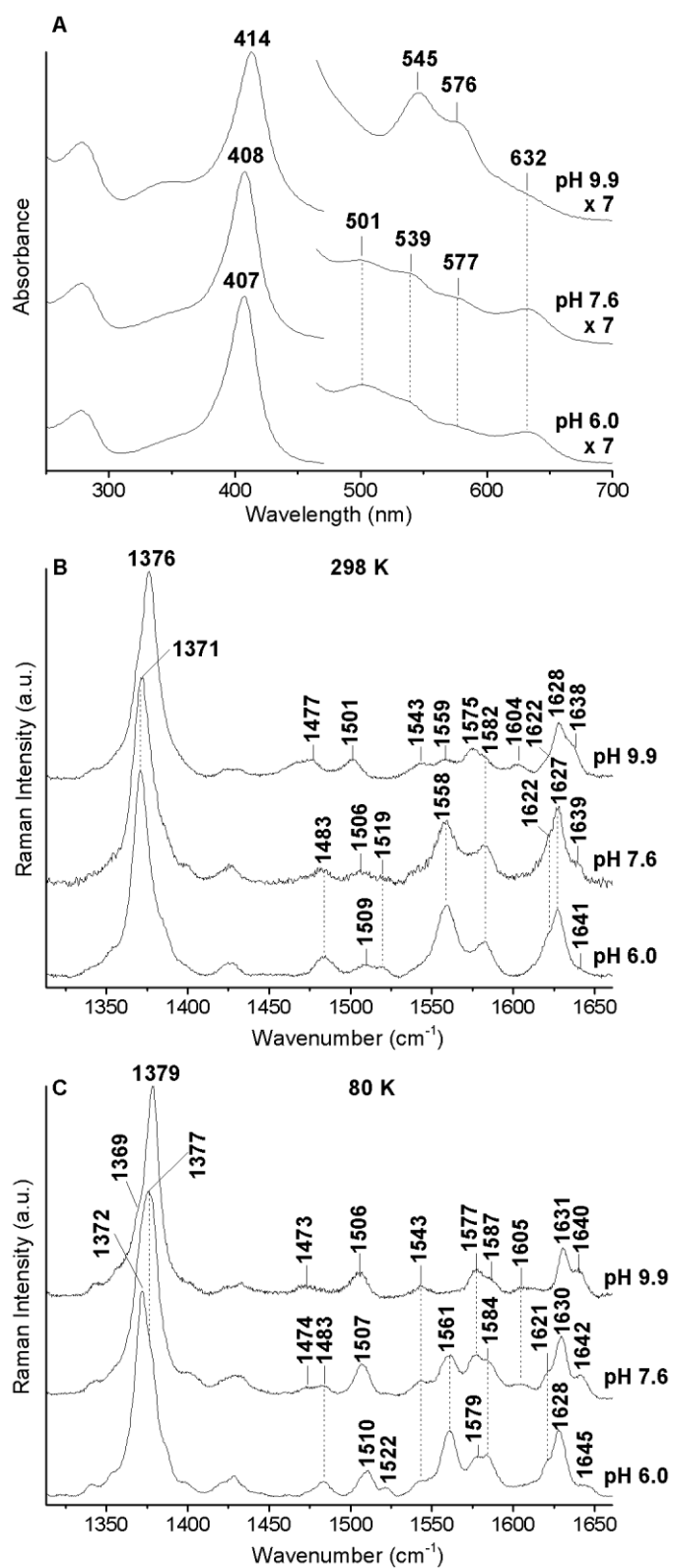
## 408 3.2. Spectroscopic characterisation

### 409 3.2.1. Ferric Form

410 **Figure 2** compares the UV-vis and the RR high-frequency region (at 298 and 80K) spectra of  
411 ferric Ph-2/2HbO-2217 at different pH. At pH 6.0, room-temperature spectra (**panels A, B**) are  
412 characteristic of a predominantly hexa-coordinate (6c) high-spin (HS) (aquo) form [charge-transfer  
413 (CT1) band at 632 nm and RR bands at 1483 ( $\nu_3$ ), 1558 ( $\nu_2$ )  $\text{cm}^{-1}$ ]. However, a weak 6c low-spin  
414 (LS) form [ $\alpha$  band at 577 nm, RR bands at 1509 ( $\nu_3$ ), 1641 ( $\nu_{10}$ )  $\text{cm}^{-1}$ ], is also present. As in Ph-  
415 2/2HbO-0030, Ph-2/2HbO-2217 undergoes an acid-alkaline transition.

416

417



418

419 **Figure 2.** Comparison of the UV-Vis (panel A) and RR spectra in the high frequency region at 298  
 420 K (panel B) and 80 K (panel C) of ferric Ph-2/2HbO-2217 at pH 6.0 (bottom), 7.6 (middle) and 9.9  
 421 (top). The spectra in all the panels have been shifted along the ordinate axis to allow better  
 422 visualisation. The 470–700-nm region of the UV-Vis spectra has been expanded 7-fold. RR

423 experimental conditions: 298 K: excitation wavelength 406.7 nm; (pH 6.0), laser power at the  
424 sample 5 mW, average of 4 spectra with 20-min integration time; (pH 7.6), laser power at the sample  
425 4 mW, using a cylindrical lens and cooling the sample with a gentle flow of N<sub>2</sub> passed through liquid  
426 N<sub>2</sub>, average of 13 spectra with 13-min integration time; (pH 9.9), excitation wavelength 413.1 nm,  
427 laser power at the sample 10 mW, average of 3 spectra with 15-min integration time; 80 K: (pH 6.0  
428 and 7.6), excitation wavelength 406.7 nm, laser power at the sample 10 mW, average of 3 spectra  
429 with 30-min integration time; (pH 9.9), excitation wavelength 413.1 nm, laser power at the sample 5  
430 mW; average of 12 spectra with 60-min integration time. The intensities of the RR spectra are  
431 normalised to that of the  $\nu_4$  band.

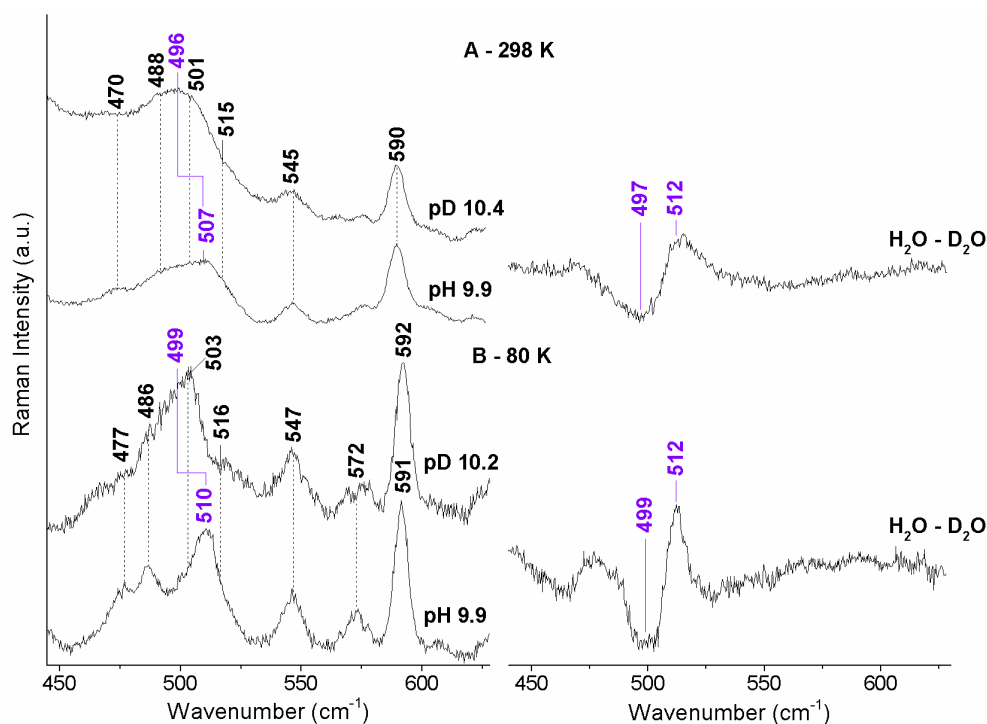
432

433 Hence, upon increasing pH, the 6cHS aquo and 6cLS forms decrease in intensity, and the new  
434 OH<sup>-</sup>-ligated forms, both 6cHS and 6cLS, grow in. At pH 9.9 (one unit lower than for Ph-2/2HbO-  
435 0030), the UV-Vis and RR spectra are typical of an OH<sup>-</sup>-ligated form, both 6cHS [1477 ( $\nu_3$ ), 1559  
436 ( $\nu_2$ ) cm<sup>-1</sup>] and 6cLS [1501( $\nu_3$ ), 1575 ( $\nu_2$ ), 1638 ( $\nu_{10}$ ) cm<sup>-1</sup>]; however, unlike for Ph-2/2HbO-0030,  
437 no 5cHS form is observed. The full assignment of the RR bands, based also on experiments carried  
438 out with excitation at 514.5 nm (**Figure S1**), is reported in Table S1.

439 The spectral dependence on pH is clearly observed in the RR spectra at low temperature  
440 (**Figure 2, panel C**). In fact, upon lowering the temperature, the sharpening of the bands and the  
441 presence of only a 6cLS OH<sup>-</sup> ligated form at alkaline pH facilitate the identification of different  
442 6cLS forms at pH 6.0 and 9.9 characterised by different RR frequencies, which are, on the other  
443 hand, both present at intermediate pH 7.6. Accordingly, in addition to a 6cHS form ( $g_{\perp} \sim 6$  and  $g_{\parallel}$   
444 2.00), the EPR spectrum at pH 7.6 (**Figure S2**) displays two 6cLS forms: one with  $g_1 = 2.95$ ,  
445 attributable to His-Fe-Tyr coordination, similar to Ph-2/2HbO-0030 (Giordano et al., 2015), and  
446 the other with  $g_1 = 2.71$ , typical of His-Fe-OH<sup>-</sup> coordination, absent in Ph-2/2HbO-0030 at pH 7.6,  
447 but present at pH 10.7 (Giordano et al., 2015).

448 **Figure 3** compares the low-frequency RR spectra of Ph-2/2HbO-2217 at alkaline pH in H<sub>2</sub>O  
 449 and D<sub>2</sub>O buffered solutions, at 298 K (**panel A, left**) and 80 K (**panel B, left**) together with the  
 450 difference spectra H<sub>2</sub>O - D<sub>2</sub>O (**Figure 3, right**).

451  
 452



453

454 **Figure 3.** Comparison of the low-frequency region RR spectra at alkaline pH of ferric Ph-2/2HbO-  
 455 2217 at room (panel A, left) and low temperature (panel B, left) in H<sub>2</sub>O (bottom) and D<sub>2</sub>O (top).  
 456 The corresponding difference spectra H<sub>2</sub>O - D<sub>2</sub>O are also shown (panels A and B, right). The  $\nu(\text{Fe-}$   
 457  $\text{OH})$  and  $\nu(\text{Fe-OD})$  mode frequencies are reported in purple. The spectra have been shifted along  
 458 the ordinate axis to allow better visualisation. The intensity of the spectra is normalised to that of  
 459 the  $\nu_4$  band. Experimental conditions: excitation wavelength 413.1 nm; pH 9.9; laser power at the  
 460 sample 10 mW, average of 9 spectra with 45-min integration time (298 K) and of 3 spectra with 60-  
 461 min integration time (80K); pD 10.2: laser power at the sample 10 mW, average of 7 spectra with  
 462 70-min integration time (298 K) and laser power at the sample 5 mW, average of 4 spectra with 40-  
 463 min integration time (80 K).

464

465 The 450-530  $\text{cm}^{-1}$  region of the spectra is quite complex, due to the porphyrin modes (see  
466 **Tables S1 and S2**). However, on the basis of the isotopic substitution, the bands at 507 and 510  
467  $\text{cm}^{-1}$  at 298 and 80 K, respectively, which shift to 496 and 499  $\text{cm}^{-1}$  in  $\text{D}_2\text{O}$  at 298 and 80 K,  
468 respectively, have been assigned to the  $\nu(\text{Fe-OH})$  mode of a His-Fe-OH<sup>-</sup> 6cLS form. Accordingly,  
469 the difference spectrum at 80 K shows narrow and well-defined bands at 499 and 512  $\text{cm}^{-1}$ . The  
470 difference spectrum at 298 K shows two broad bands at 497 and 512  $\text{cm}^{-1}$ , possibly due to the  
471 concomitant presence of a His-Fe-OH<sup>-</sup> 6cHS form observed at room temperature in the RR high-  
472 frequency region (**Figure 2, panel B**). The frequency of the Ph-2/2HbO-2217  $\nu(\text{Fe-OH})$  mode is  
473 about 18 and 46  $\text{cm}^{-1}$  lower than that observed for Ph-2/2HbO-0030 (525  $\text{cm}^{-1}$  at 298 K, Giordano  
474 et al., 2015) and human Hb (553  $\text{cm}^{-1}$  at 298 K, Feis et al., 1994), indicating the presence of strong  
475 H-bonds between the OH<sup>-</sup> ligand and distal residues. In fact, with an increase of the H-bond  
476 strength, a decrease of the force constant of the Fe-OH bond, with concomitant decrease of the  
477  $\nu(\text{Fe-OH})$  stretching frequency, is expected. However, no upshift of the frequency is observed in  
478  $\text{D}_2\text{O}$ , as in Ph-2/2HbO-0030 (543  $\text{cm}^{-1}$ , Giordano et al., 2015) or other heme proteins in the  
479 presence of strong H-bonds (Nicoletti et al., 2014; Howes et al., 2015). Moreover, due to the  
480 instability of Ph-2/2HbO-2217 in  $\text{H}_2^{18}\text{O}$  buffer, the identification of any  $\nu(\text{Fe-OH})$  band on the  
481 basis of its sensitivity to  $^{18}\text{O}$  substitution was not possible.

482 Therefore, in general, the spectroscopic features of ferric Ph-2/2HbO-0030 and Ph-2/2HbO-  
483 2217 are similar, the main differences being the lower  $\text{pK}_a$  for the alkaline transition (about one unit)  
484 of Ph-2/2HbO-2217 compared to Ph-2/2HbO-0030, and the absence of a 5cHS form in Ph-2/2HbO-  
485 2217 at alkaline pH. Accordingly, the low-frequency regions of the RR spectra of the two proteins  
486 are also very similar (**Figure S3**). The only notable differences concern the frequency and/or  
487 intensity of the vinyl and propionyl bending modes. The  $\delta(\text{C}_\beta\text{C}_a\text{C}_b)$  bending modes of the vinyl  
488 groups of Ph-2/2HbO-2217 give rise to a broad band centered at 415  $\text{cm}^{-1}$ , 5  $\text{cm}^{-1}$  higher than in Ph-  
489 2/2HbO-0030. At present, the significance of these variations is not clear, but they possibly suggest

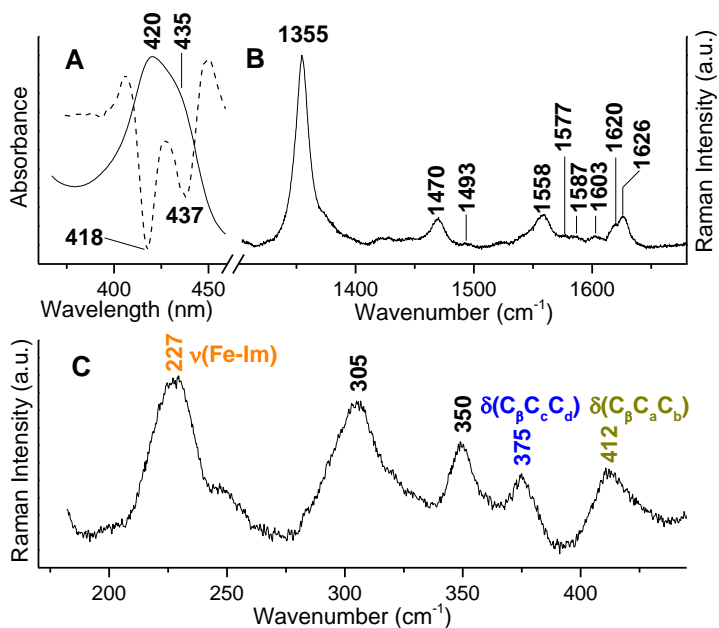
490 differences in vinyl orientation, in agreement with the  $3\text{-cm}^{-1}$  difference of the  $\nu(\text{C}=\text{C})$  stretching  
491 modes (Smulevich et al., 1996; Marzocchi and Smulevich, 2003).

492 The relative intensity of the  $\delta(\text{C}_\beta\text{C}_\alpha\text{C}_\delta)$ -propionyl bending modes is markedly different. In  
493 particular, the propionyl mode at  $381\text{ cm}^{-1}$  is more intense in Ph-2/2HbO-2217 than in Ph-2/2HbO-  
494 0030. This behaviour is observed also in the ferrous carbonylated complex (see below). The  
495 frequency and intensity of this mode has been correlated with the hydrogen-bond strength between  
496 the heme-propionate and the nearby residues (Cerdeira-Còlon et al., 1998). As suggested by the  
497 different primary structure of the residues surrounding the heme propionyls, the intensity change of  
498 one propionyl mode indicates that the H-bonding interactions are different for the two proteins, and  
499 in particular much stronger in Ph-2/2HbO-2217.

500

### 501 3.2.2. Ferrous Form

502 Upon reduction, the UV-Vis and RR high-frequency-region spectra of Ph-2/2HbO-2217  
503 clearly reveal the presence of a 6cLS form (Soret band at 420 nm and RR bands at 1493 ( $\nu_3$ ), 1577  
504 ( $\nu_2$ )  $\text{cm}^{-1}$ ) and a 5cHS form (Soret band at 435 nm and RR bands at 1470 ( $\nu_3$ ), 1558 ( $\nu_2$ ) and 1603  
505 ( $\nu_{10}$ )  $\text{cm}^{-1}$ ), (**Figure 4**), the latter being much more pronounced in Ph-2/2HbO-2217 than Ph-  
506 2/2HbO-0030 (**Figure S4**). The RR low-frequency-region spectrum of Ph-2/2HbO-2217 is  
507 characterised by a very strong band at  $227\text{ cm}^{-1}$ , assigned to the  $\nu(\text{Fe-Im})$  stretching mode (**Figure**  
508 **4**). The frequency of this band is  $5\text{-cm}^{-1}$  higher than in Ph-2/2HbO-0030 ( $222\text{ cm}^{-1}$ ) (Giordano et  
509 al., 2011), indicating a stronger proximal Fe-His bond. The frequency is similar to that of other  
510 2/2Hbs (Egawa and Yeh, 2005), consistent with a staggered orientation of the imidazole ring of the  
511 proximal His with respect to the four pyrrole nitrogen atoms of the porphyrin ring, revealed by the  
512 crystallographic data of Ph-2/2HbO-0030 (Giordano et al., 2015), in contrast to the eclipsed  
513 orientation observed in human Hb.



514

515 **Figure 4.** UV-Vis and its the second derivative spectrum ( $D^2$ ) (dashed line) (panel A), RR spectra in  
 516 the high- (panel B) and low-frequency region (panel C) of ferrous Ph-2/2HbO-2217 at pH 7.6. The  
 517 spectra have been shifted along the ordinate axis to allow better visualisation. In panel C the  $\nu(\text{Fe-Im})$ ,  
 518  $\delta(\text{C}_\beta\text{C}_c\text{C}_d)$  and  $\delta(\text{C}_\beta\text{C}_a\text{C}_b)$  mode frequencies are reported in orange, blue and green,  
 519 respectively. RR experimental conditions: excitation wavelength 441.6 nm; laser power at the  
 520 sample 10 mW, average of 4 spectra with 20-min integration time.

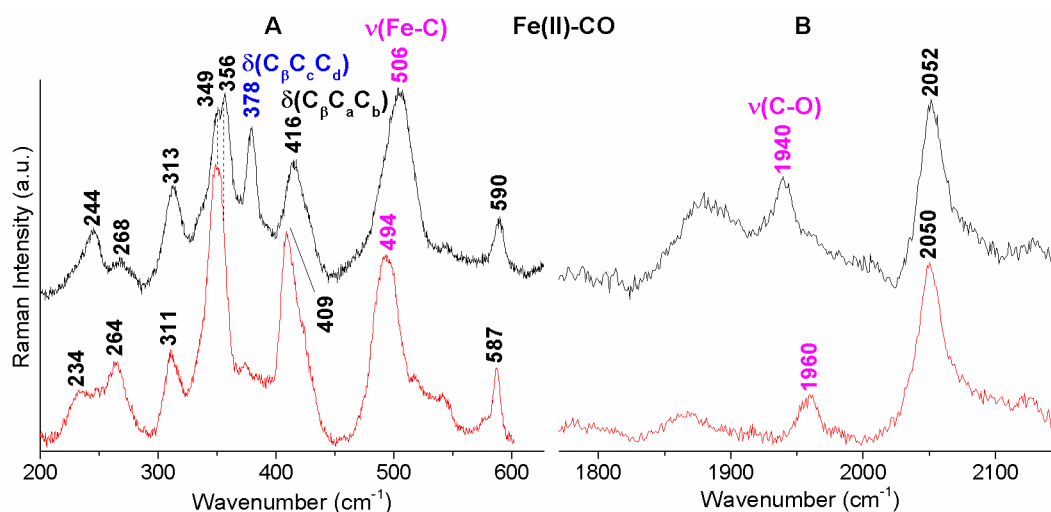
521

522 Moreover, similar to the ferric form, slight differences compared to Ph-2/2HbO-0030 are  
 523 evident in the vinyl stretching ( $1624\text{-}1626\text{ cm}^{-1}$ ) and bending ( $409, 412\text{ cm}^{-1}$ ) modes.

524 As in Ph-2/2HbO-0030 (Giordano et al., 2011), Ph-2/2HbO-2217 binds CO, giving rise to a  
 525  $6c\text{LS}$  species. In the RR low-frequency region of the CO adduct (**Figure 5, panel A**), one isotope-  
 526 sensitive band is identified in both Ph-2/2HbO-0030 ( $494\text{ cm}^{-1}$ ) and Ph-2/2HbO-2217 ( $506\text{ cm}^{-1}$ ),  
 527 which shift to  $489$  and  $501\text{ cm}^{-1}$ , respectively, in the case of  $^{13}\text{CO}$  (**Figure S5**). These bands are  
 528 assigned to the  $\nu(\text{Fe-C})$  stretching mode. Accordingly, a corresponding  $\nu(\text{C-O})$  stretching mode is  
 529 observed at  $1960\text{ cm}^{-1}$  (Ph-2/2HbO-0030) and  $1940\text{ cm}^{-1}$  (Ph-2/2HbO-2217) (**Figure 5, panel B**),  
 530 which shift to  $1914\text{ cm}^{-1}$  and  $1898\text{ cm}^{-1}$ , respectively, upon  $^{13}\text{CO}$  substitution (**Figure S5**).

531





532

533 **Figure 5.** Comparison of the RR spectra of the Fe(II)-<sup>12</sup>CO complexes of Ph-2/2HbO-0030 (red) and  
 534 Ph-2/2HbO-2217 (black) at pH 7.6. The low (panel A) and the high (panel B) frequency regions  
 535 show the  $\nu(\text{Fe-CO})$  and  $\nu(\text{C-O})$  stretching modes (in magenta), respectively. The  $\delta(\text{C}_\beta\text{C}_\gamma\text{C}_\delta)$  mode  
 536 frequency is shown in blue. The spectra have been shifted along the ordinate axis to allow better  
 537 visualisation. RR experimental conditions: excitation wavelength 413.1 nm; a cylindrical lens was  
 538 used to focus the laser beam on the sample; laser power at the sample 2 mW, average of 4 spectra  
 539 with 10-min integration time (Ph-2/2HbO-0030, LF and HF); laser power at the sample 2 mW,  
 540 average of 3 spectra with 30-min integration time (Ph-2/2HbO-2217, LF); average of 9 spectra with  
 541 90-min integration time (Ph-2/2HbO-2217, HF).

542

543 Interestingly, unlike ferrous carbonylated Ph-2/2HbO-0030 CO, whose frequencies are  
 544 characteristic of a CO conformer in which polar interactions with the surrounding residues of the  
 545 distal cavity are absent, the corresponding CO frequencies for the Ph-2/2HbO-2217 CO complex  
 546 indicate polar interactions between the distal residues and the CO molecule. This finding is  
 547 consistent also with the presence of strong H-bonds between the OH<sup>-</sup> ligand and distal residues, not  
 548 observed for Ph-2/2HbO-0030. Furthermore, the frequency shifts and marked intensity increase of  
 549 the  $\delta(\text{C}_\beta\text{C}_\gamma\text{C}_\delta)$ -propionate bands upon formation of the CO-complex suggest a change in the  
 550 environment around the propionate group in Ph-2/2HbO-2217 when the hexa-coordinated species is

551 formed. This is likely consequent to a marked strengthening of the H-bonding interactions between  
552 the heme propionates and the nearby residues. Interestingly, in Ph-2/2HbO-0030, CO binding causes  
553 the complete disappearance of the propionyl bending modes (**Figure 3**), indicating changes in the  
554 strength of hydrogen bonding from moderate to weak upon formation of the CO-complex. These  
555 observations suggest a flexible heme rocking motion that contributes to the ligand-binding  
556 mechanism in the two proteins that might also be influenced by the different H-bonding residues in  
557 the vicinity of the propionates for Ph-2/2HbO-2217 and Ph-2/2HbO-0030.

558

559 3.3. Cloning and expression of the PSHAa2217 gene in E. coli TOP10 cells and in the hmp mutant

560 The PSHAa2217 gene from PhTAC125 was cloned into the commercial vector pBAD/HisA  
561 (Invitrogen, Carlsbad, CA, USA), under control of an L-arabinose-inducible promoter. The construct  
562 pBAD-2/2HbO-2217 was confirmed by sequencing, and later expressed both in E. coli TOP10 cells  
563 to purify the protein, and in the E. coli hmp mutant to perform in vivo function experiments. Since  
564 the mutant is very sensitive to NO and RNS, complementation in trans of sensitivity indicates that  
565 the expressed globin is endowed with detoxification properties. Expression resulted in the  
566 accumulation of heme protein inside the cell, giving a reddish brown colour to the recombinant E.  
567 coli cells. SDS-PAGE demonstrated the presence of a ~15.5-kDa protein corresponding to the  
568 expected size of Ph-2/2HbO-2217. Ph-2/2HbO-2217, cloned and over-expressed in E. coli TOP10,  
569 was purified by two consecutive anion-exchange chromatography steps (**Figure S6, panels A-B**). In  
570 agreement with the primary structure of Ph-2/2HbO-2217, a ~15.5-kDa protein was obtained  
571 (**Figure S6, insert C**).

572 To confirm the expression of the PSHAa2217 gene in E. coli hmp, the UV-visible absorption  
573 spectrum of lysate of the cells carrying pBAD-2/2HbO-2217 was compared with that of cells  
574 transformed with the empty vector pBAD/HisA (**Figure S7**).

575

576 3.4 Growth of the NO-sensitive E. coli hmp strain carrying Ph-2/2HbO-2217 under nitrosative stress

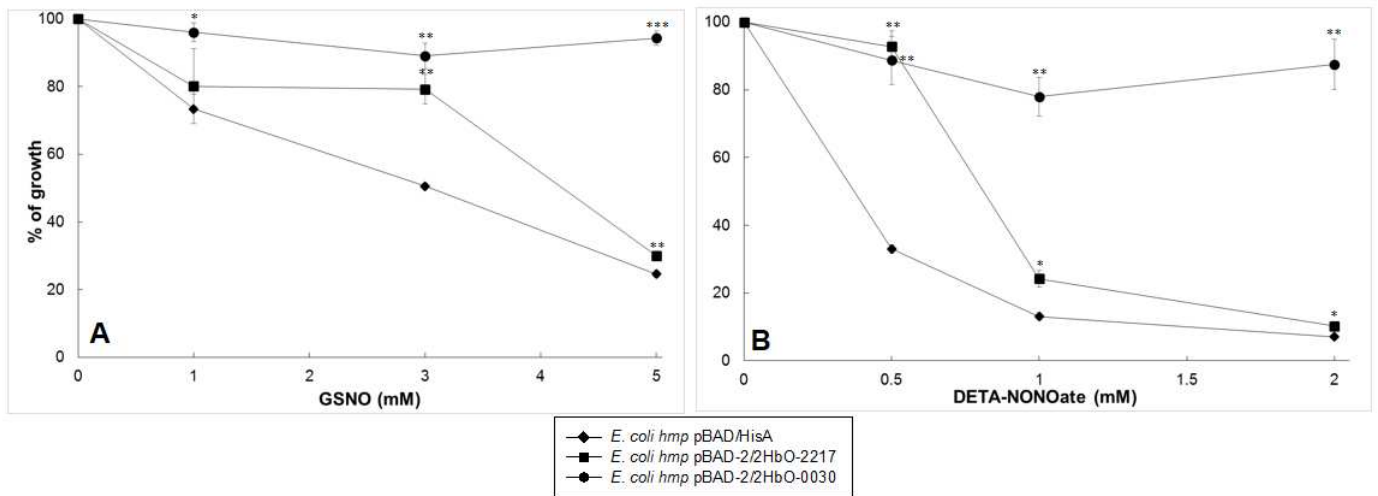
577 The putative role of the globin Ph-2/2HbO-2217 was investigated in vivo using the *E. coli hmp*  
578 mutant to identify NO-detoxification mechanisms. *E. coli hmp* cells carrying Ph-2/2HbO-2217 were  
579 grown overnight with induction supplements at 25 °C, in the absence and presence of increasing  
580 concentrations of either the nitrosating agent GSNO (0, 1, 3, and 5 mM) (**Figure 6A**) or of the NO-  
581 releaser DETA-NONOate (0, 0.5, 1, and 2 mM) (**Figure 6B**). The slightly higher concentrations  
582 required for GSNO than for DETA-NONOate activity presumably reflect the fact that GSNO  
583 releases only low levels of NO (Bowman et al., 2011; Laver et al., 2012) that is detoxified by  
584 globins. In fact, 500 μM GSNO releases less NO than 5 μM DEA-NONOate, a relatively fast-  
585 releasing NO-donor liberating 1.5 mol per mol parent compound (Jarboe et al., 2008).

586 The effect of the expression of the PSHAa2217 gene (**Figure 6**) on the ability of *E. coli hmp*  
587 cells to survive in the presence of nitrosative stress was compared to that of cultures of *E. coli hmp*  
588 transformed with pBAD/HisA (negative control), or pBAD-2/2HbO-0030 (positive control)  
589 (Coppola et al., 2013).

590 The growth of the *hmp* mutant was progressively inhibited at all GSNO and DETA-NONOate  
591 concentrations tested (up to 5 mM GSNO and 2 mM DETA-NONOate). However, exposure to  
592 nitrosative stress had no effect on the growth of *E. coli hmp* cells expressing Ph-2/2HbO-0030  
593 (Coppola et al., 2013), reflecting complete restoration of NO-detoxifying properties endowed by the  
594 FHb. The growth of the *E. coli hmp* mutant carrying the PSHAa2217 gene was also significantly  
595 improved relative to the un-complemented mutant, at 3 mM GSNO (**Figure 6A**) or 0.5 mM DETA-  
596 NONOate (**Figure 6B**). These data demonstrate the involvement of both cold-adapted globins in  
597 protecting the heterologous host from NO toxicity.

598 The protein encoded by the PSHAa2217 gene appeared less efficient in protection from  
599 nitrosative stress compared to Ph-2/2HbO-0030. However, we cannot exclude the possibility that the  
600 lower efficiency of the Ph-2/2HbO-2217 compared to Ph-2/2HbO-0030 may be due to different  
601 levels of expression of these globins. The heme content in the cells carrying the PSHAa0030 gene  
602 was around 2-fold higher than that of *E. coli hmp* carrying the PSHAa2217 gene.

603



604

605 **Figure 6.** Susceptibility test of *E. coli hmp* expressing different plasmids supplemented with GSNO  
606 (A) and DETA-NONOate (B). Cultures of *E. coli hmp* carrying pBAD-2/2HbO-2217 after addition  
607 of 0.2 mM  $\delta$ -aminolevulinic acid, 0.012 mM FeCl<sub>3</sub>, 0.06% L-arabinose (squares), were grown for 18  
608 h at 25 °C under aerobic conditions, and the optical density was recorded. The same strain, carrying  
609 pBAD/HisA (diamonds) and pBAD-2/2HbO-0030 (circles), grown in the presence of 0.2% and  
610 0.06% L-arabinose, respectively, were included as controls. Values are means  $\pm$  standard deviation.  
611 Errors bars of standard deviation were calculated by experiments carried out in triplicate. The  
612 significance of the data (*E. coli hmp* expressing Ph-2/2HbO-2217 and Ph-2/2HbO-0030 compared to  
613 *E. coli hmp* with pBAD/HisA) was estimated with a Student's t-test. \*\*\*P<0.001; \*\*P<0.01;  
614 \*P<0.05.

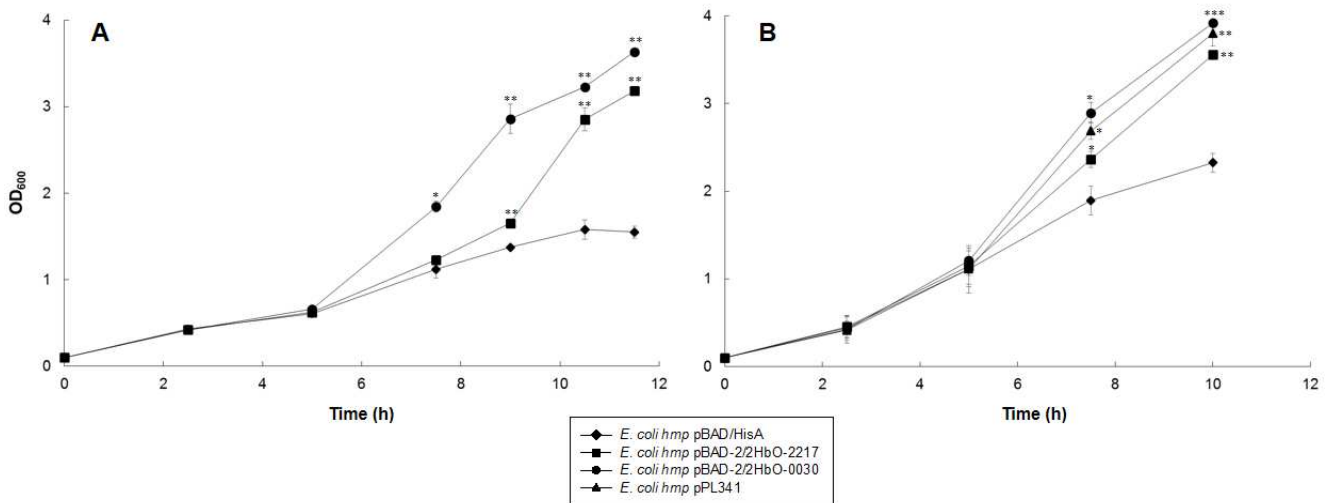
615

616 To confirm these results and demonstrate that, similar to Ph-2/2HbO-0030, Ph-2/2HbO-2217  
617 also confers resistance during growth, cultures of the *E. coli hmp* mutant, carrying pBAD-2/2HbO-  
618 2217, pBAD/HisA, or pBAD-2/2HbO-0030, were grown at 25 °C under aerobic conditions and  
619 treated with either 3 mM GSNO (Figure 7A) or 0.5 mM DETA-NONOate (Figure 7B).

620 In the presence of GSNO, the ability of cells expressing Ph-2/2HbO-2217 to grow under  
621 nitrosative stress was also compared to that of cultures of *E. coli hmp* transformed with the plasmid

622 carrying the wild-type *hmp*<sup>+</sup> gene from plasmid pPL341 (**Figure 7B**), as an additional positive  
623 control (Coppola et al., 2013).

624



625

626 **Figure 7.** Growth profile of *E. coli hmp* expressing Ph-2/2HbO-2217 (squares), Ph-2/2HbO-0030  
627 (circles), pBAD/HisA (diamonds), and pPL341 (triangles, Fig. 7B only), exposed to 3.0 mM GSNO  
628 (A) and 0.5 mM DETA-NONOate (B). Cultures were grown at 25 °C, under aerobic conditions, and  
629 supplemented with 0.2 mM  $\delta$ -aminolevulinic acid, 0.012 mM FeCl<sub>3</sub>, L-arabinose at the final  
630 concentration of 0.06% for *E. coli hmp* carrying either Ph-2/2HbO-2217, the empty vector or  
631 pPL341, and at the final concentration of 0.2% for the positive control *E. coli hmp* carrying Ph-  
632 2/2HbO-0030. Values are means  $\pm$  standard deviation. Errors bars of standard deviation were  
633 calculated by experiments carried out in triplicate. The significance of the data (*E. coli hmp*  
634 expressing Ph-2/2HbO-2217 and Ph-2/2HbO-0030 compared to *E. coli hmp* with pBAD/HisA) was  
635 estimated with a Student's t-test. \*\*\*P<0.001; \*\*P<0.01; \*P<0.05.

636

637 Exposure to GSNO caused a slight decrease in growth of the *E. coli hmp* mutant carrying  
638 pBAD-2/2HbO-2217 compared to the mutant carrying Ph-2/2HbO-0030. In contrast, the growth  
639 profile of negative control cells bearing the empty vector pBAD/HisA was drastically reduced.  
640 Similar results were obtained in the presence of DETA-NONOate, even if the Antarctic globins

641 seem to be more effective in protecting growth from inhibition by DETA-NONOate than from  
642 GSNO. This may reflect the more complex toxic effects of GSNO (especially nitrosation reactions)  
643 (Laver et al., 2012) than NO. It is worth noting that globins detoxify NO but not GSNO per se  
644 (Laver et al., 2012). In the case of the NONOate, the complete alleviation of growth inhibition by  
645 expressing pPL341 encoding the E. coli flavohaemoglobin Hmp, is clear.

646 Altogether, these results demonstrate that the globin Ph-2/2HbO-2217 provides substantial  
647 protection to the cells from NO toxicity in the heterologous host.

648

### 649 3.5. NO consumption and respiration rate of E. coli hmp expressing the PSHAa2217 gene

650 We noted that expression of Ph-2/2HbO-2217 was lower in the hmp mutant than that of Ph-  
651 2/2HbO-0030 and so, to eliminate the possibility that this contributed to interpreting measurements  
652 of growth and respiration in the presence of nitrosative stress agents, we performed experiments with  
653 suspensions of harvested cells in which protein and heme levels were quantified. Cells were grown  
654 at 25 °C in the presence of the induction supplements and under aerobic conditions and the  
655 respiration of E. coli hmp cells carrying the PSHAa2217 gene, the PSHAa0030 gene, or the empty  
656 vector, exposed to NO toxicity, was measured. Because GSNO is a poor NO donor (Jarboe et al.,  
657 2008) and is not a potent inhibitor of cell respiration, the course of O<sub>2</sub> and NO consumption was  
658 measured in the presence and absence of the fast NO-releaser Proli-NONOate (**Figure 8**). The  
659 toxicity of NO depends on O<sub>2</sub> concentration (Stevanin et al., 2000); thus, additions of NO were made  
660 at three different O<sub>2</sub> tensions after stimulating respiration by adding 25 mM glucose. At each NO  
661 addition, revealed by a rapid upward excursion of the NO electrode output, the O<sub>2</sub> uptake was  
662 abruptly stopped but resumed when the NO levels fell. When NO decreased to a minimal level,  
663 respiration continued until the chamber became anaerobic. In the absence of NO, all three strains  
664 consumed O<sub>2</sub> at a similar rate when respiration was normalised to total cell protein content, as  
665 assessed in the Markwell assay (6.4-8.4 nmol O<sub>2</sub>/min/mg) (Markwell et al., 1978). However, when  
666 respiration rates were expressed relative to heme content, the strains expressing the globins showed

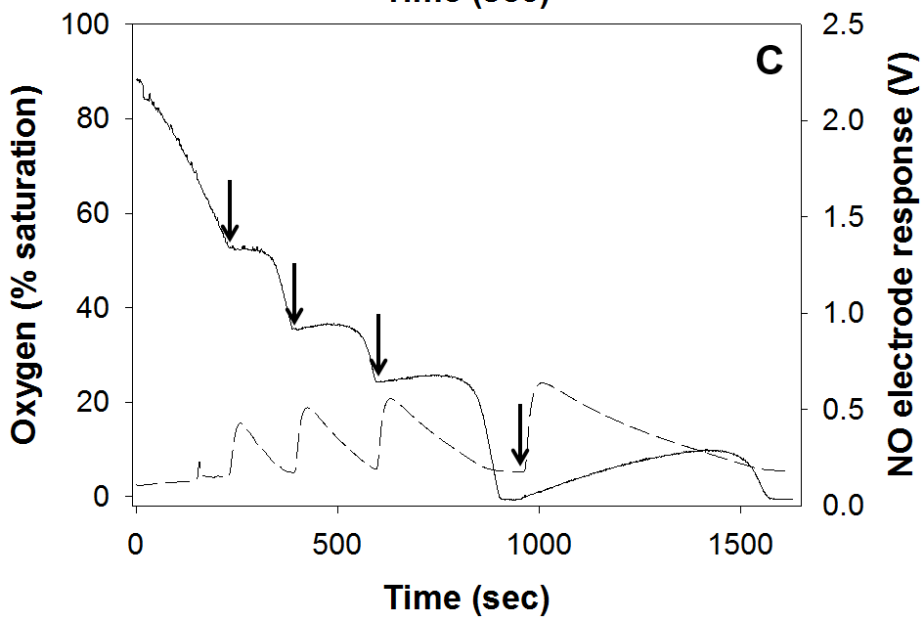
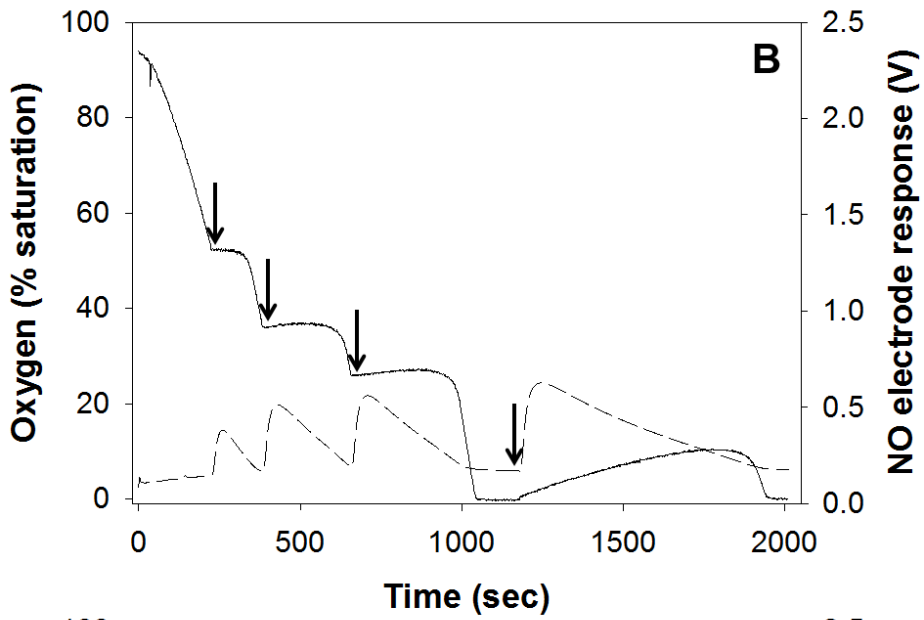
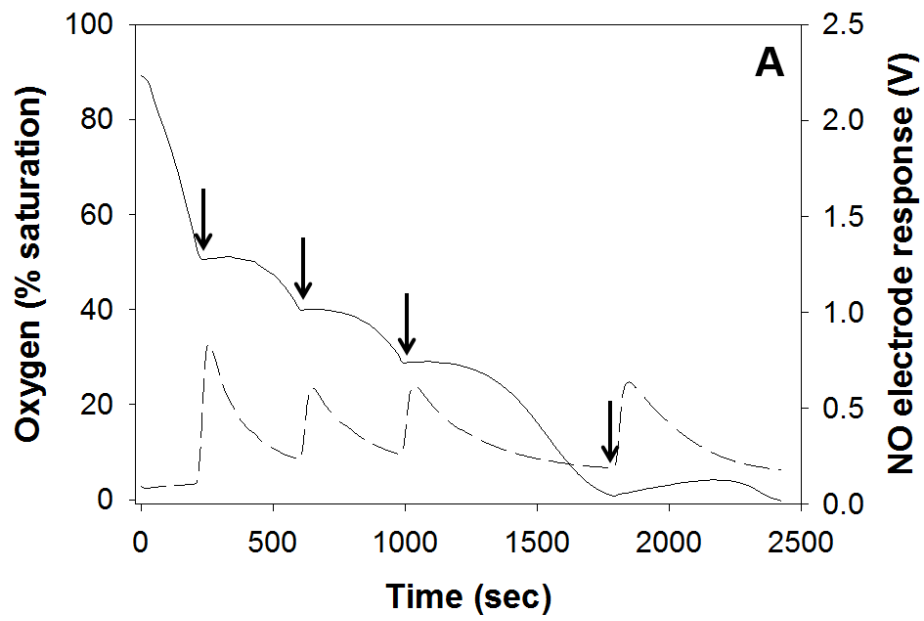
667 significantly lower respiration rates (6-10 nmol O<sub>2</sub>/min/mM heme) than the strain containing the  
668 control pBAD/HisA plasmid (15 nmol O<sub>2</sub>/min/mM heme); this reflects the lack of globin-catalysed  
669 O<sub>2</sub> uptake in the absence of NO.

670 To assess the roles of the two globins in NO detoxification, we measured the rates of O<sub>2</sub> uptake  
671 after each NO addition and expressed this relative to the pre-NO rates of O<sub>2</sub> uptake. In Figure 8A,  
672 the rate before adding NO (49 nmol O<sub>2</sub>/min) was severely reduced by successive NO additions.  
673 After each addition there was a transient, almost complete, inhibition of respiration, but activity  
674 resumed as the NO concentration declined (as shown by the NO electrode traces). However, the  
675 rates never regained the pre-NO rates: in Figure 8A, three successive NO additions resulted in  
676 inhibition of >65-73% of the pre-NO rate. In marked contrast, in the case of the two globin-  
677 expressing strains (Figure 8B, C), the resumption of O<sub>2</sub> uptake after NO additions regained  
678 completely the pre-NO rates and, indeed, an acceleration of O<sub>2</sub> uptake. In the case of Ph-2/2HbO-  
679 2217, the observed rates were 1.5-2.1-fold higher than the pre-NO rate and in the case of Ph-  
680 2/2HbO-0030, the observed rates were 1.2-1.7-fold higher than the pre-NO rate.

681 We have already reported the ability of the *E. coli* hmp strain carrying the PSHAa0030 gene to  
682 detoxify NO (Coppola et al., 2013); the present data show that both globins are able to restore  
683 respiration to pre-NO rates. We attribute the final stimulation of respiration to the globin-catalysed  
684 reaction between the remaining NO and O<sub>2</sub>. When O<sub>2</sub> was depleted, further additions of NO resulted  
685 in a larger NO signal and in its slower disappearance (**Figure 8A-C**), indicating O<sub>2</sub>-dependent NO  
686 consumption.

687 Taken together, these results indicate that Ph-2/2HbO-2217, like Ph-2/2HbO-0030, is able to  
688 restore O<sub>2</sub> consumption in vitro after NO challenge, and probably involved in the bacterial defence  
689 against nitrosative stress.

690





692 **Figure 8.** NO uptake and respiration of *E. coli* hmp carrying either the empty vector (pBAD/HisA)  
693 (A) or expressing Ph-2/2HbO-0030 (B), or Ph-2/2HbO-2217 (C). Respiration was followed in a  
694 Clark-type O<sub>2</sub> electrode (solid traces) upon additions of 1 μM Proli-NONOate (arrows). NO uptake  
695 was measured simultaneously with an NO electrode (dashed traces). After inhibition of respiration  
696 by the last aliquot of NO, the slight upward deflections of the O<sub>2</sub> traces probably reflect either the  
697 polarographic drift or the back-diffusion of O<sub>2</sub> into the chamber through the Hamilton syringe used  
698 to make NO additions. All experiments were performed in triplicate. The volumes of cell  
699 suspensions used were adjusted to give similar O<sub>2</sub> uptake rates in the absence of NO.

700

### 701 3.6. Peroxynitrite isomerisation

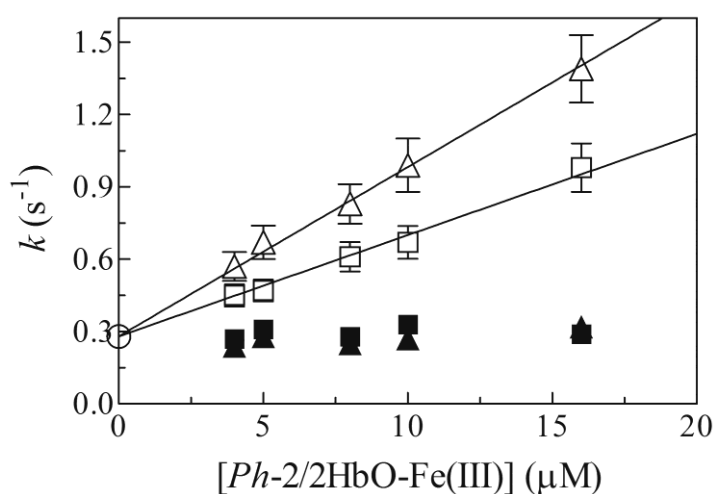
702 As shown in **Figure 9**, ferric Ph-2/2HbO-2217 catalyses peroxynitrite isomerisation, as  
703 reported for several globins, e.g. horse heart Mb (Herold and Shivashankar, 2003). On the other  
704 hand, cyanide-bound ferric Ph-2/2HbO-2217 does not facilitate peroxynitrite isomerisation, as  
705 previously reported in hexa-coordinated heme-proteins, e.g. human neuroglobin (Herold et al.,  
706 2004b) and horse heart cytochrome c (Ascenzi et al., 2011a, b), showing high affinity with  
707 intramolecular distal ligands.

708 Under all the experimental conditions, the time course of peroxynitrite conversion to nitrate is  
709 a monophasic process for more than 87% of its course. As shown in **Figure 9**, the first-order rate  
710 constant  $k$  increases linearly with the concentration of ferric Ph-2/2HbO-0030 and Ph-2/2HbO-  
711 2217. The analysis of data shown in **Figure 9** according to Eq. 2 allowed the determination of the  
712  $k_{on}$  and  $k_0$  values for peroxynitrite conversion to nitrate by the ferric globins. The values of  $k_{on}$   
713 (corresponding to the slope of the linear plot) are  $4.0 \times 10^4 \text{ M}^{-1} \text{ s}^{-1}$  and  $7.2 \times 10^4 \text{ M}^{-1} \text{ s}^{-1}$  for Ph-  
714 2/2HbO-2217- and Ph-2/2HbO-0030-mediated isomerisation of peroxynitrite, respectively, at pH  
715 7.4 and 20 °C.

716 The y intercept of the linear plot corresponds to  $0.28 \text{ s}^{-1}$ , matching with  $k_0$  values ( $0.30 \text{ s}^{-1}$ )  
717 obtained either in the absence of both ferric globins or in the presence of unreactive ferric globin-  
718 cyanide adducts.

719 Interestingly, values of  $k_{\text{on}}$  for peroxynitrite scavenging by Ph-2/2HbO-2217 and Ph-2/2HbO-  
720 0030 are similar to those reported for sperm whale Mb and human Hb (Herold and Shivashankar,  
721 2003), representing the major targets of RNS in vivo (Herold and Fago, 2005).

722



723

724 **Figure 9.** Dependence of  $k$  for peroxynitrite isomerization on the concentration of ferric Ph-  
725 2/2HbO-2217, in the absence and presence of cyanide (open and filled squares, respectively). Data  
726 for peroxynitrite isomerisation by ferric Ph-2/2HbO-0030 in the absence and presence of cyanide  
727 (open and filled triangles, respectively) are reported for comparison. All data were obtained at pH  
728 7.4 and  $20 \text{ }^\circ\text{C}$ . The circle on the ordinate indicates the value of  $k$  in the absence of globins. The  
729 continuous lines were calculated according to Eq. 2 with  $k_{\text{on}} = 4.0 \times 10^4 \text{ M}^{-1} \text{ s}^{-1}$  (squares) and  
730  $7.2 \times 10^4 \text{ M}^{-1} \text{ s}^{-1}$  (triangles), and  $k_0 = 0.28 \text{ s}^{-1}$ . In the presence of saturating cyanide ( $5.0 \times 10^{-4} \text{ M}$ ),  
731 values of  $k$  are independent of the ferric-globin concentration and the average value of  $k = 0.30 \text{ s}^{-1}$   
732 corresponds to that of  $k_0$  (circle). The peroxynitrite concentration was  $2.5 \times 10^{-5} \text{ M}$ . When not  
733 shown, the standard deviation is smaller than the symbol. For details, see text.

734

735 **4. Discussion**

736 Life at low temperature imposes a wide array of challenges to marine bacteria. At low  
737 temperatures, the enhanced O<sub>2</sub> solubility significantly increases the production rate of ROS.  
738 Therefore, bacteria must be able to adjust to temperature changes and availability of nutrients. A  
739 genome analysis of *Colwellia psychroerythraea* (Méthé et al., 2005) and *Desulfotalea psychrophila*  
740 (Rabus et al., 2004) suggests that a common strategy to face environmental challenges consists of  
741 developing enhanced antioxidant capacity, resulting from multiple genes that encode catalases and  
742 superoxide dismutases.

743 By contrast, in silico analysis of the PhTAC125 genome (Médigue et al., 2005) suggests that  
744 this Antarctic marine bacterium may cope with increased O<sub>2</sub> solubility by multiplying O<sub>2</sub>-  
745 scavenging enzymes (such as dioxygenases) and deleting entire metabolic pathways that generate  
746 ROS as side products. Moreover, its resistance to H<sub>2</sub>O<sub>2</sub> is due to the presence of several enzymes  
747 involved in scavenging chemical groups affected by ROS (such as peroxiredoxins and peroxidases),  
748 and one catalase-encoding gene (*katB*) and a possible homologue (*PSHAa1737*) (Médigue et al.,  
749 2005).

750 Furthermore, in order to prevent significant damage to cellular structures, PhTAC125  
751 improves the redox buffering capacity of the cytoplasm, and glutathione synthetase is strongly up-  
752 regulated at low temperature (Piette et al., 2010). These adjustments in antioxidant defenses are  
753 needed to maintain the steady-state concentration of ROS and may be important components in  
754 evolutionary adaptations in cold and O<sub>2</sub>-rich environments. In fact, PhTAC125 is able to thrive in  
755 pelagic form, where cells experience a high concentration of O<sub>2</sub> and other gases that characterise  
756 cold waters. In addition, although the strain thrives between 2 and 4 °C, it is also able to survive  
757 long-term frozen conditions when entrapped in the winter sea ice (Médigue et al., 2005).

758 The presence of multiple globin genes in distinct positions on chromosome I of PhTAC125  
759 (Giordano et al., 2007) may be pivotal for cell protection. To our knowledge, PhTAC125 is the first  
760 example of coexistence of genes encoding a FHb and three 2/2Hbs (Giordano et al., 2013), of which

761 both Ph-2/2HbO-0030 and Ph-2/2HbO-2217 are endowed with hexa-coordination (Giordano et al.,  
762 2011; Howes et al., 2011; Russo et al., 2013; Giordano et al., 2015; this study). Endogenous hexa-  
763 coordination may be essential for proteins that function under high levels of oxidative stress  
764 (Johnson and Lecomte, 2013).

765         When complementing this study with our earlier work (Coppola et al., 2013), it appears that  
766 both Ph-2/2HbO-2217 and Ph-2/2HbO-0030 provide protection against NO and related reactive  
767 species, under aerobic conditions. At first sight, two hexa-coordinated globins capable of  
768 performing NO detoxification appear redundant. However, variations in physico-chemical features  
769 of the marine environment may require diversified responses, which may be reflected in appropriate  
770 modulation of gene expression in this bacterium. Our incomplete knowledge of the physiological  
771 role of the two globins, which is probably multifaceted, is another aspect that needs to be  
772 considered. For example, the genome of many fish species can express multiple Hbs having similar  
773 Bohr and Root effects, which points to apparently similar mechanisms in O<sub>2</sub> binding and release.

774         Transcriptional analysis of the genes encoding globins in PhTAC125 wild type and in the  
775 PhTAC125-0030 mutant showed that the transcription of the FHb-encoding gene (PSHAa2880)  
776 was observed in the PhTAC125-0030 mutant when grown at 4 °C in microaerobiosis (Parrilli et al.,  
777 2010). Since the transcription of FHb-encoding genes is linked to globin-mediated NO  
778 detoxification (Membrillo-Hernández et al., 1999; Mills et al., 2001; Stevanin et al., 2000), the  
779 observed FHb-gene expression is suggestive of the occurrence of NO-induced stress intimately  
780 correlated to the absence of Ph-2/2HbO-0030. Although the PhTAC125 genome contains two  
781 additional 2/2Hbs encoding genes, transcribed in all the experimental conditions tested in Parrilli et  
782 al. (2010), mutation of the gene encoding Ph-2/2HbO-0030 is sufficient to obtain a strain with a  
783 clear mutant phenotype. This suggests that the numerous globins in this bacterium are not  
784 functionally redundant in PhTAC125 physiology.

785         The high reactivity of the ferric forms of Ph-2/2HbO-0030 (Coppola et al., 2013) and Ph-  
786 2/2HbO-2217 towards peroxynitrite suggests that protection against RNS and ROS is a strong need

787 in the cold Antarctic environment. Low temperatures are known to decrease nitrate uptake among  
788 bacteria, and nitrogen is fundamental for bacteria replication and synthesis of proteins.

789 Several procedures were attempted to purify the expressed Ph-2/2HbO-2217 to  
790 homogeneity, but they were unsuccessful thus precluding the possibility to determine its physico-  
791 chemical properties under physiological conditions. Therefore, two in vivo and in vitro models have  
792 been developed to highlight the protective role of Ph-2/2HbO-2217 against RNS. However, the  
793 nitrosative stress-sensitive *E. coli* is protected from NO by ferrous Ph-2/2HbO-2217, which is  
794 involved in O<sub>2</sub>- and NO-consumption (**Figures 6, 7 and 8**), and ferric Ph-2/2HbO-2217 which  
795 catalyses in vitro peroxynitrite scavenging (**Figure 9**). These results suggest that ferrous and ferric  
796 Ph-2/2HbO-2217 could be involved in the detoxification of RNS (i.e., NO and peroxynitrite,  
797 respectively), thus protecting the bacterium from these nitrosative stress mechanisms.

798 The main features of Ph-2/2HbO-2217 and Ph-2/2HbO-0030 are the presence of a longer  
799 sequence extension of the N-terminal region (19 residues in Ph-2/2HbO-0030 and 9 residues in Ph-  
800 2/2HbO-2217), that in Ph-2/2HbO-0030 is proteolytically cleaved during protein purification  
801 (Giordano et al., 2007), and does not appear to reduce the NO scavenging activity (Coppola et al.,  
802 2013). Pesce et al. (2016) have recently demonstrated that removal of the pre-A region in *M.*  
803 tuberculosis Mt-2/2HbN promotes the assembly of a stable dimer, both in the crystals and in  
804 solution, hypothesising that the pre-A region may be essential for survival of the microorganism  
805 because it significantly reduces the ability of Mt-2/2HbN to scavenge NO by interfering with ligand  
806 diffusion. Accordingly, kinetic measurements of Mt-2/2HbN-DpreA indicate that the  $k_{on}$  values for  
807 peroxynitrite isomerisation by the mutant protein were four-fold lower than in the wild-type protein  
808 (Pesce et al., 2016).

809 Interestingly, also 2/2HbI, encoded by the PSHAa0458 gene in the PhTAC125 genome, is  
810 characterised by an extension at the N terminus longer than that observed in Mt-2/2HbN; from  
811 preliminary results, the protein shows endogenous hexa-coordination (Daniela Giordano, personal  
812 communication), similar to the other genes of 2/2Hbs present in the genome of PhTAC125.

813           Although transcriptional regulation is the main mechanism in stress responses, regulation of  
814 translation is faster and consequently very important for species. Post-transcriptional regulation  
815 occurs at different stages and includes generation of proteins that need to be activated to perform  
816 their function (Varshavsky, 2011). The strategy allows cells to respond quickly to environmental  
817 stimuli by simply activating preexistent proteins. We cannot exclude that these extensions at the N  
818 terminus may play a role in the native host, namely the Antarctic bacterium, although the  
819 experiments performed by Coppola et al. (2013) in the mutant of *E. coli* as heterologous host did  
820 not show any involvement of the pre-A region of Ph-2/2HbO-0030 in NO detoxification.  
821 Altogether, these findings indicate the need of PhTAC125 to quickly react to the environment by  
822 implementing proteins that function under high levels of oxidative stress.

823

#### 824 **Acknowledgements**

825 This study is in the framework of the SCAR programme “Antarctic Thresholds - Ecosystem  
826 Resilience and Adaptation” (AnT-ERA). It was financially supported by the Italian National  
827 Programme for Antarctic Research (PNRA). We are grateful to two anonymous Reviewers, whose  
828 comments and suggestions greatly helped us to improve the quality of this paper.

829

830

831

832

833 **References**

834

835 [Arnold K, Bordoli L, Kopp J, Schwede T \(2006\) The SWISS-MODEL workspace: a web-based](#)  
836 [environment for protein structure homology modelling. \*Bioinformatics\*, 22, 195-201.](#)

837 Ascenzi P, Fasano M (2007) Abacavir modulates peroxynitrite-mediated oxidation of ferrous  
838 nitrosylated human serum heme-albumin. *Biochem. Biophys. Res. Commun.* 353, 469-474.

839 Ascenzi P, De Marinis E, Visca P, Ciaccio C, Coletta M (2009) Peroxynitrite detoxification by  
840 ferryl *Mycobacterium leprae* truncated hemoglobin O. *Biochem. Biophys. Res. Commun.* 380,  
841 392-6.

842 Ascenzi P, Ciaccio C, Sinibaldi F, Santucci R, Coletta M (2011a) Cardiolipin modulates  
843 allosterically peroxynitrite detoxification by horse heart cytochrome c. *Biochem. Biophys.*  
844 *Res. Commun.* 404, 190-194.

845 Ascenzi P, Ciaccio C, Sinibaldi F, Santucci R, Coletta M (2011b) Peroxynitrite detoxification by  
846 horse heart carboxymethylated cytochrome c is allosterically modulated by cardiolipin.  
847 *Biochem. Biophys. Res. Commun.* 415, 463-467.

848 Ascenzi P, di Masi A, Tundo GR, Pesce A, Visca P, Coletta M (2014) Nitrosylation mechanisms of  
849 *Mycobacterium tuberculosis* and *Campylobacter jejuni* truncated hemoglobins N, O, and P.  
850 *PLoS One.* 9, e102811.

851 [Benkert P, Biasini M, Schwede T \(2011\) Toward the estimation of the absolute quality of individual](#)  
852 [protein structure models. \*Bioinformatics\*, 27, 343-350.](#)

853 [Biasini M, Bienert S, Waterhouse A, Arnold K, Studer G, Schmidt T, Kiefer F, Gallo Cassarino T,](#)  
854 [Bertoni M, Bordoli L, Schwede T \(2014\) SWISS-MODEL: modelling protein tertiary and](#)  
855 [quaternary structure using evolutionary information. \*Nucleic Acids Res.\* 42: W252-8.](#)

856 Bohle DS, Glassbrenner PA, Hansert B (1996) Syntheses of pure tetramethylammonium  
857 peroxynitrite. *Methods Enzymol.* 269, 302-311.

858 Bonamore A, Ilari A, Giangiacomo L, Bellelli A, Morea V, Boffi A (2005) A novel thermostable  
859 hemoglobin from the actinobacterium *Thermobifida fusca*. *FEBS J.* 272, 4189-4201.

860 Boubeta FM, Bari SE, Estrin DA, Boechi L (2016) Access and binding of H<sub>2</sub>S to heme proteins: the  
861 case of HbI of *Lucina pectinata*. *J. Phys. Chem. B.* 120, 9642-9653.

862 Bowman LA, McLean S, Poole RK, Fukuto J (2011) The diversity of microbial responses to nitric  
863 oxide and agents of nitrosative stress: close cousins but not identical twins. *Adv. Microb.*  
864 *Physiol.* 59, 135–219.

865 Bustamante JP, Radusky L, Boechi L, Estrin DA, Ten Have A, Martí MA (2016) Evolutionary and  
866 functional relationships in the truncated hemoglobin family. *PLoS Comput.* \_

867 Cerda-Còlon JF, Silfa E, Lopez-Garriga J (1998) Unusual rocking freedom of the heme in the  
868 hydrogen sulfide-binding hemoglobin from *Lucina pectinata*. *J. Am. Chem. Soc.* 120, 9312-  
869 9317.

870 Ciaccio C, Tognaccini L, Battista T, Cervelli M, Howes BD, Santucci R, Coletta M, Mariottini P,  
871 Smulevich G, Fiorucci L (2017) The Met80Ala and Tyr67His/Met80Ala mutants of human  
872 cytochrome c shed light on the reciprocal role of Met80 and Tyr67 in regulating ligand access  
873 into the heme pocket. *J. Inorg. Biochem.* 169, 86-96.

874 Coppola D, Giordano D, Tinajero-Trejo M, di Prisco G, Ascenzi P, Poole RK, Verde C (2013)  
875 Antarctic bacterial hemoglobin and its role in the protection against nitrogen reactive species.  
876 *Biochim. Biophys. Acta.* 1834, 1923-1931.

877 Crowe SA, Døssing LN, Beukes NJ, Bau M, Kruger SJ, Frei R, Canfield DE (2013) Atmospheric  
878 oxygenation three billion years ago. *Nature.* 501, 535-538.

879 De Marinis E, Casella L, Ciaccio C, Coletta M, Visca P, Ascenzi P (2009) Catalytic peroxidation of  
880 nitrogen monoxide and peroxyxynitrite by globins. *IUBMB Life.* 61, 62-73.

881 Egawa T, Yeh SR (2005) Structural and functional properties of hemoglobins from unicellular  
882 organisms as revealed by resonance Raman spectroscopy. *J. Inorg. Biochem.* 99, 72-96.



883 Feis A, Marzocchi MP, Paoli M, Smulevich G (1994) Spin state and axial ligand bonding in the  
884 hydroxide complexes of metmyoglobin, methemoglobin, and horseradish peroxidase at room  
885 and low temperatures. *Biochemistry*. 33, 4577-4583.

886 Gardner PR, Gardner AM, Martin LA, Salzman AL (1998) Nitric oxide dioxygenase: an enzymic  
887 function for flavohemoglobin. *Proc. Natl. Acad. Sci. USA*. 95, 10378–10383.

888 Gardner PR (2005) Nitric oxide dioxygenase function and mechanism of flavohemoglobin,  
889 hemoglobin, myoglobin and their associated reductases. *J. Inorg. Biochem*. 99, 247-266.

890 Giangiacomo A, Ilari L, Boffi A, Morea V, Chiancone E (2005) The truncated oxygen-avid  
891 hemoglobin from *Bacillus subtilis*: X-ray structure and ligand binding properties. *J. Biol.*  
892 *Chem*. 280, 9192-9202.

893 Giordano D, Parrilli E, Dettai A, Russo R, Barbiero G, Marino G, Lecointre G, di Prisco G, Tutino  
894 ML, Verde C (2007) The truncated hemoglobins in the Antarctic psychrophilic bacterium  
895 *Pseudoalteromonas haloplanktis* TAC125. *Gene*. 398, 69-77.

896 Giordano D, Russo R, Ciaccio C, Howes BD, di Prisco G, Marden MC, Hui Bon Hoa G, Smulevich  
897 G, Coletta M, Verde C (2011) Ligand- and proton-linked conformational changes of the  
898 ferrous 2/2 hemoglobin of *Pseudoalteromonas haloplanktis* TAC125. *IUBMB Life*. 63, 566-  
899 573.

900 Giordano D, Coppola D, Russo R, Tinajero-Trejo M, di Prisco G, Lauro F, Ascenzi P, Verde C  
901 (2013) The globins of cold-adapted *Pseudoalteromonas haloplanktis* TAC125: from the  
902 structure to the physiological functions. *Adv. Microb. Physiol*. 63, 329-389.

903 Giordano D, Pesce A, Boechi L, Bustamante JP, Caldelli E, Howes BD, Riccio A, di Prisco G,  
904 Nardini M, Estrin D, Smulevich G, Bolognesi M, Verde C (2015) Structural flexibility of the  
905 heme cavity in the cold adapted truncated hemoglobin from the Antarctic marine bacterium  
906 *Pseudoalteromonas haloplanktis* TAC125. *FEBS J*. 282, 2948-2965.

907 Giovannoni SJ, Tripp HJ, Givan S, Podar M, Vergin KL, Baptista D, Bibbs L, Eads J, Richardson  
908 TH, Noordewier M, Rappé MS, Short JM, Carrington JC, Mathur EJ (2005) Genome  
909 streamlining in a cosmopolitan oceanic bacterium. *Science*. 309, 1242-1245.

910 Goldstein S, Merényi G (2008) The chemistry of peroxyxynitrite: implications for biological activity.  
911 *Methods Enzymol*. 436, 49-61.

912 Jarboe LR, Hyduke DR, Tran LM, Chou KJ, Liao JC (2008) Determination of the *Escherichia coli*  
913 S-nitrosoglutathione response network using integrated biochemical and systems analysis. *J.*  
914 *Biol. Chem*. 283, 5148-5157.

915 Johnson EA, Lecomte JT (2013) The globins of cyanobacteria and algae. *Adv. Microb. Physiol*. 63,  
916 195-272.

917 Hart TW (1985) Some observations concerning the S-nitroso and S-phenylsulphonyl derivatives of  
918 L-cysteine and glutathione. *Tetrahedron Lett*. 26, 2013-2016.

919 Herold S, Shivashankar K (2003) Metmyoglobin and methemoglobin catalyze the isomerization of  
920 peroxyxynitrite to nitrate. *Biochemistry*. 42, 14036-14046.

921 Herold S, Kalinga S, Matsui T, Watanabe Y (2004a) Mechanistic studies of the isomerization of  
922 peroxyxynitrite to nitrate catalyzed by distal histidine metmyoglobin mutants. *J. Am. Chem. Soc*.  
923 126, 6945-6955.

924 Herold S, Fago A, Weber RE, Dewilde S, Moens L (2004b) Reactivity studies of the Fe(III) and  
925 Fe(II)NO forms of human neuroglobin reveal a potential role against oxidative stress. *J. Biol.*  
926 *Chem*. 279, 22841-22847.

927 Herold S, Fago A (2005) Reactions of peroxyxynitrite with globin proteins and their possible  
928 physiological role. *Comp Biochem Physiol A Mol Integr Physiol*. 142, 124-129

929 Howes BD, Giordano D, Boechi L, Russo R, Mucciacciaro S, Ciaccio C, Sinibaldi F, Fittipaldi M,  
930 Martí MA, Estrin DA, di Prisco G, Coletta M, Verde C, Smulevich G (2011) The peculiar  
931 heme pocket of the 2/2 hemoglobin of cold adapted *Pseudoalteromonas haloplanktis* TAC125.  
932 *J. Biol. Inorg. Chemistry*. 16, 299-311.

933 Howes BD, Boechi L, Boffi A, Estrin DA, Smulevich G (2015) Bridging theory and experiment to  
934 address structural properties of truncated haemoglobins: Insights from *Thermobifida fusca*  
935 HbO. In *Adv. Microb. Physiol. Recent Advances in Microbial Oxygen-binding Proteins*  
936 (Poole RK, Ed.) Vol. 67, 85-126.

937 Kalnenieks U, Galinina N, Kalnenieks U, Galinina N, Bringer- Meyer S, Poole RK (1998)  
938 Membrane D-lactate oxidase in *Zymomonas mobilis*: evidence for a branched respiratory  
939 chain. *FEMS Microbiol. Lett.* 168, 91–97.

940 Koppenol WH, Kissner R, Beckman JS (1996) Syntheses of peroxynitrite: to go with the flow or on  
941 solid grounds? *Methods Enzymol.* 269, 296-302.

942 Ilari A, Kjelgaard P, von Wachenfeldt C, Catacchio B, Chiancone E, Boffi A (2007) Crystal  
943 structure and ligand binding properties of the truncated hemoglobin from *Geobacillus*  
944 *stearothermophilus*. *Arch. Biochem. Biophys.* 457, 85-94.

945 Laver JR, McLean S, Bowman LA, Harrison LJ, Read RC, Poole RK (2012) Nitrosothiols in  
946 bacterial pathogens and pathogenesis. *Antioxid. Redox Signal.* 18, 309-322.

947 Markwell MA, Haas SM, Bieber LL, Tolbert NE (1978) A modification of the Lowry procedure to  
948 simplify protein determination in membrane and lipoprotein samples. *Anal. Biochem.* 87, 206-  
949 210.

950 Marzocchi MP, Smulevich G (2003) Relationship between heme vinyl conformation and the protein  
951 matrix in peroxidases. *J. Raman Spectrosc.* 34, 725-736.

952 Médigue C, Krin E, Pascal G, Barbe V, Bernsel A, Bertin PN, Cheung F, Cruveiller S, D'Amico S,  
953 Duilio A, Fang G, Feller G, Ho C, Mangenot S, Marino G, Nilsson J, Parrilli E, Rocha EP,  
954 Rouy Z, Sekowska A, Tutino ML, Vallenet D, von Heijne G, Danchin A (2005) Coping with  
955 cold: the genome of the versatile marine Antarctica bacterium *Pseudoalteromonas*  
956 *haloplanktis* TAC125. *Genome Res.* 15, 1325-1335.

957 Membrillo-Hernández J, Coopamah MD, Anjum MF, Stevanin TM, Kelly A, Hughes MN, Poole  
958 RK (1999) The flavohemoglobin of *Escherichia coli* confers resistance to a nitrosating agent,

959 a “nitric oxide releaser”, and paraquat and is essential for transcriptional responses to  
960 oxidative stress. *J. Biol. Chem.* 274, 748-754.

961 Methé BA, Nelson KE, Deming JW, Momen B, Melamud E, Zhang X, Moulton J, Madupu R, Nelson  
962 WC, Dodson RJ, Brinkac LM, Daugherty SC, Durkin AS, DeBoy RT, Kolonay JF, Sullivan  
963 SA, Zhou L, Davidsen TM, Wu M, Huston AL, Lewis M, Weaver B, Weidman JF, Khouri H,  
964 Utterback TR, Feldblyum TV, Fraser CM (2005) The psychrophilic lifestyle as revealed by the  
965 genome sequence of *Colwellia psychrerythraea* 34H through genomic and proteomic analyses.  
966 *Proc. Natl. Acad. Sci. USA.* 102, 10913-10918.

967 Milani M, Savard PY, Ouellet H, Ascenzi P, Guertin M, Bolognesi M (2003) A TyrCD1/TrpG8  
968 hydrogen bond network and a TyrB10TyrCD1 covalent link shape the heme distal site of  
969 *Mycobacterium tuberculosis* hemoglobin O. *Proc Natl Acad Sci USA.* 100, 5766–5771.

970 Milani M, Pesce A, Nardini M, Ouellet H, Ouellet Y, Dewilde S, Bocedi A, Ascenzi P, Guertin M,  
971 Moens L, Friedman JM, Wittenberg JB, Bolognesi M (2005) Structural bases for heme  
972 binding and diatomic ligand recognition in truncated hemoglobins. *J. Inorg. Biochem.* 99, 97-  
973 109.

974 Mills CE, Sedelnikova S, Søballe B, Hughes MN, Poole RK (2001) *Escherichia coli*  
975 flavohaemoglobin (Hmp) with equistoichiometric FAD and haem contents has a low affinity  
976 for dioxygen in the absence or presence of nitric oxide. *Biochem. J.* 353, 207-213.

977 Nardini M, Pesce A, Milani M, Bolognesi M (2007) Protein fold and structure in the truncated (2/2)  
978 globin family. *Gene.* 398, 2-11.

979 Nicoletti FP, Bustamante JP, Droghetti E, Howes BD, Fittipaldi M, Bonamore A, Baiocco P, Feis  
980 A, Boffi A, Estrin DA, Smulevich G (2014) Interplay of the H-bond donor–acceptor role of  
981 the distal residues in hydroxyl ligand stabilization of *Thermobifida fusca* truncated  
982 hemoglobin. *Biochemistry.* 53, 8021-8030.

983 Parrilli E, Giuliani M, Giordano D, Russo R, Marino G, Verde C, Tutino ML (2010) The role of a  
984 2-on-2 haemoglobin in oxidative and nitrosative stress resistance of Antarctic  
985 *Pseudoalteromonas haloplanktis* TAC125. *Biochimie*. 92, 1003-1009.

986 Pesce A, Nardini M, Labarre M, Richard C, Wittenberg JB, Wittenberg BA, Guertin M, Bolognesi  
987 M (2011) Structural characterization of a group II 2/2 hemoglobin from the plant pathogen  
988 *Agrobacterium tumefaciens*. *Biochim. Biophys. Acta*. 1814, 810-816.

989 Pesce A, Bolognesi M, Nardini M (2013) The diversity of 2/2 (truncated) globins. *Adv. Microb.*  
990 *Physiol.* 63, 49-78.

991 Pesce A, Bustamante JP, Bidon-Chanal A, Boechi L, Estrin DA, Luque FJ, Sebilo A, Guertin M,  
992 Bolognesi M, Ascenzi P, Nardini M (2016) The N-terminal pre-A region of *Mycobacterium*  
993 *tuberculosis* 2/2HbN promotes NO-dioxygenase activity. *FEBS J.* 283, 305-322.

994 Piette F, D'Amico S, Struvay C, Mazzucchelli G, Renaut J, Tutino ML, Danchin A, Leprince P,  
995 Feller G (2010) Proteomics of life at low temperatures: trigger factor is the primary chaperone  
996 in the Antarctic bacterium *Pseudoalteromonas haloplanktis* TAC125. *Mol. Microbiol.* 76,  
997 120-132.

998 Rabus R, Ruepp A, Frickey T, Rattei T, Fartmann B, Stark M, Bauer M, Zibat A, Lombardot T,  
999 Becker I, Amann J, Gellner K, Teeling H, Leuschner WD, Glöckner FO, Lupas AN, Amann  
1000 R, Klenk HP (2004) The genome of *Desulfotalea psychrophila*, a sulfate-reducing bacterium  
1001 from permanently cold Arctic sediments. *Environ. Microbiol.* 6, 887-902.

1002 Russo R, Giordano D, di Prisco G, Hui Bon Hoa G, Marden MC, Verde C, Kiger L (2013) Ligand  
1003 rebinding kinetics of 2/2 hemoglobin from the Antarctic bacterium *Pseudoalteromonas*  
1004 *haloplanktis* TAC125. *Biochim. Biophys. Acta*. 1834, 1932-1938.

1005 Smulevich G, Hu S, Rodgers KR, Goodin DB, Smith KM, Spiro TG (1996) Heme-protein  
1006 interactions in CCP revealed by site-directed mutagenesis and Resonance Raman spectra of  
1007 isotopically labeled hemes. *Biospectroscopy* 2, 365-376.

1008 Stevanin TM, Ioannidis N, Mills CE, Kim SO, Hughes MN, Poole RK (2000) Flavohemoglobin  
1009 Hmp affords inducible protection for Escherichia coli respiration, catalyzed by cytochromes  
1010 bo' or bd, from nitric oxide. *J. Biol. Chem.* 275, 35868-35875.

1011 Vasudevan SG, Armarego WL, Shaw DC, Lilley PE, Dixon NE, Poole RK (1991) Isolation and  
1012 nucleotide sequence of the hmp gene that encodes a haemoglobin-like protein in Escherichia  
1013 coli K-12. *Mol. Gen. Genet.* 226, 49-58.

1014 Visca P, Fabozzi G, Petrucca A, Ciaccio C, Coletta M, De Sanctis G, Bolognesi M, Milani M,  
1015 Ascenzi P (2002) The truncated hemoglobin from Mycobacterium leprae. *Biochem. Biophys.*  
1016 *Res. Commun.* 294, 1064-1070.

1017 Vinogradov SN, Hoogewijs D, Bailly X, Arredondo-Peter R, Gough J, Dewilde S, Moens L,  
1018 Vanfleteren JR (2006) A phylogenomic profile of globins. *BMC Evol. Biol.* 6, 31.

1019 Vinogradov S, Tinajero-Trejo M, Poole RK, Hoogewijs D (2013) Bacterial and archaeal globins - A  
1020 revised perspective. *Biochim. Biophys. Acta.* 1834, 1789-1800.

1021 Vuletich DA, Lecomte JT (2006) A phylogenetic and structural analysis of truncated hemoglobins.  
1022 *J. Mol. Evol.* 62, 196-210.

1023 Varshavsky A (2011) The N-end rule pathway and regulation by proteolysis. *Protein Sci.* 20, 1298-  
1024 1345.

1025 Wittenberg JB, Bolognesi M, Wittenberg BA, Guertin M (2002) Truncated hemoglobins: A new  
1026 family of hemoglobins widely distributed in bacteria, unicellular eukaryotes, and plants. *J.*  
1027 *Biol. Chem.* 227, 871-874.

1028